frontiers | Frontiers in Nanotechnology

TYPE Original Research
PUBLISHED 23 July 2025
DOI 10.3389/fnano.2025.1595252

OPEN ACCESS

EDITED BY
Xiaoyu Gao,
Baylor University, United States

REVIEWED BY
Mohamed S. Moawad,
Baylor University, United States
Jon Beard,
Baylor University, United States
Raja Muthuramalingam Thangavelu,
Connecticut Agricultural Experiment Station, United States

*CORRESPONDENCE
Anuj Rana,
anujrana@hau.ac.in
Rahul Kumar Dhaka,
rahulkdhaka@hau.ac.in

RECEIVED 17 March 2025
ACCEPTED 26 May 2025
PUBLISHED 23 July 2025

CITATION
Kumar P, Rana A, Sheokand M, Kumar S, Chaudhary K, Nandal U, Kumar S and Dhaka RK (2025) Biofortification and growth enhancement of wheat via bacteria-assisted iron and zinc nanoparticles.
Front. Nanotechnol. 7:1595252.
doi: 10.3389/fnano.2025.1595252

Biofortification and growth enhancement of wheat via bacteria-assisted iron and zinc nanoparticles

Pradeep Kumar[1], Anuj Rana[1]*, Mansi Sheokand[2], Suresh Kumar[3], Kautilya Chaudhary[4], Urvashi Nandal[5], Sandeep Kumar[6] and Rahul Kumar Dhaka[2]*

[1]Department of Microbiology, College of Basic Sciences and Humanities, CCS Haryana Agricultural University, Hisar, India, [2]Department of Chemistry, College of Basic Sciences and Humanities, CCS Haryana Agricultural University, Hisar, India, [3]Department of Agronomy, College of Agriculture, CCS Haryana Agricultural University, Hisar, India, [4]Department of Soil Science, College of Agriculture, CCS Haryana Agricultural University, Hisar, India, [5]Department of Foods and Nutrition, IC College of Community Science, CCS Haryana Agricultural University, Hisar, India, [6]Department of Physics, Punjab Engineering College (Deemed to be University), Chandigarh, India

This study reports the isolation of four bacteria from metal-enriched sites and rhizosphere soil and evaluated their tolerance (to 9 mM) toward iron (ferric chloride) and zinc (zinc sulfate). Among all the four isolates, AW5 exhibited plant growth-promoting (PGP) traits, namely, siderophores, indole-3-acetic acid, and increased solubilization of zinc and phosphorus. AW5 efficiently synthesized iron and zinc nanoparticles (NPs) of size 135 nm and 197 nm, respectively. The biologically synthesized iron and zinc NPs (20 ppm) enhanced the bacteria (AW5) growth, production of indole-3-acetic acid and siderophore, and solubilization of phosphate and zinc. A combination of plant growth-promoting rhizobacteria (PGPR) and NPs (seed priming) significantly improved shoot (up to 9%) and root length (up to 35%), wheat dry biomass (up to 96%), 100-grain weight (up to 28%), iron content (14%), and zinc content (4%) versus the recommended dose of fertilizer (RDF) control under a pot experiment. A foliar spray of NPs combined with PGPR seed priming showed a significant increase in shoot length (7%) and root length (up to 14%), wheat dry biomass (up to 59%), 100-grain weight (up to 34%), iron content (27%), and zinc content (53%) versus the RDF control under a pot experiment. Nanoparticle treatment through seed priming or foliar spray enhanced plant growth hormones (auxin, 59%) and chlorophyll A and B (51% and 107%) and soil microbial enzymes (dehydrogenase up to 53% and fluorescein diacetate up to 164%), and increased grain fat (65%) and ash content (42%). The synthesized NPs improved root morphology, photosynthesis, and soil enzymatic activities that enhanced the availability of micronutrients from soil to plant for its growth and biofortification. The synergistic impact of NPs bolstered plant–bacteria interactions, hence increasing nutrient uptake by improving the root architecture and facilitating the availability of FeNPs and ZnNPs. This study provides valuable insights into employing bacteria-assisted NPs in biofortification and crop productivity to achieve agricultural sustainability.

KEYWORDS

iron and zinc nanoparticles, plant growth-promoting rhizobacteria, bacterial synthesis, wheat biofortification, sustainable agriculture, nanobiofertilizer

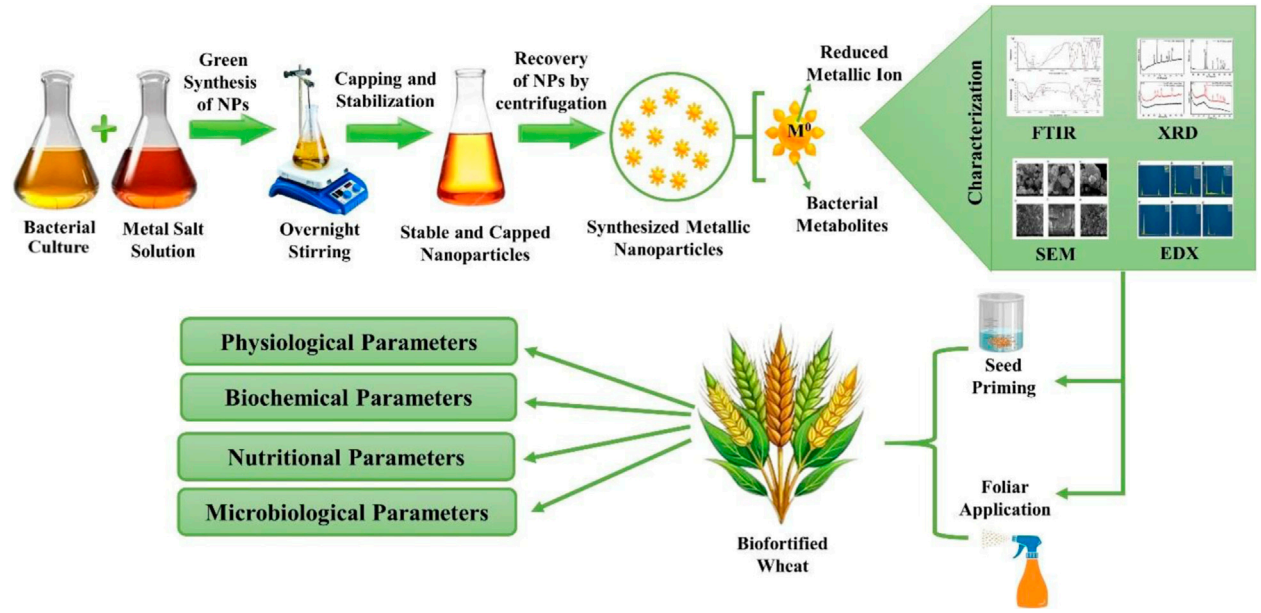

GRAPHICAL ABSTRACT
Bacterial synthesis, characterization and application of Fe and Zn NPs for wheat crop biofortification and productivity.

1 Introduction

Modern agricultural practices have rendered the soil deficient in organic carbon and resulted in the poor availability of nutrients. Cereal crops are widely cultivated and consumed as a staple food to ensure food security and nutrition for the ever-increasing global population. Innovative organic formulations rich in available nutrients must be devised. Nanotechnology can play an important role in formulating and developing sustainable agri-inputs for prolonged release to provide nutrients to plants for better growth, quality, and yield (Kumar et al., 2025). The synthesis of NPs through biological methods has become attractive due to their environmentally friendly nature versus chemical approaches (Campaña et al., 2023).

A biological approach involving microorganisms for nanoparticle (NP) synthesis provides biocompatible material. A diverse range of NPs (geometric and metallic) was biosynthesized using organisms like bacteria, fungi, yeasts, and plants (Shankar et al., 2016; Rana et al., 2020). The microbial synthesis of NPs is mediated by enzymes, proteins, and other biomolecules secreted by the microorganism. These biological agents reduce metal salts to oxides to attain compatibility via active, passive, or combined mechanisms (Khan et al., 2020). The approach of NP synthesis and modification via microbial agents is simple, sustainable, and economically viable (Mukherjee et al., 2001; Ahmad et al., 2003) with a possibility to achieve controlled size and shape (Iqtedar et al., 2020; Guardiola-Márquez et al., 2023). Zinc oxide and iron oxide nanoparticles have been widely used in the agricultural and allied sectors (Chatterjee et al., 2011; Zhang et al., 2021; Guardiola-Márquez et al., 2023).

Nanoparticles significantly impact the interactions between microorganisms and plants, leading to improved plant growth, nutrient uptake, and stress tolerance. The integration of NPs into agricultural systems holds great promise for enhancing microbial growth and promoting plant–microbe interactions (Shukla et al., 2015). Iron (Fe) and zinc (Zn) oxide NPs have stimulated the growth and activity of plant growth-promoting rhizobacteria (PGPR). They have also served as carriers for PGPR, protecting them in harsh environmental conditions and facilitating their attachment to plant roots (Chatterjee et al., 2011; Liu et al., 2013; Timmusk et al., 2018). Nanotechnology-based delivery methods have improved the efficacy of agricultural inputs, alleviated environmental concerns, and enhanced sustainability in agriculture (González-Melendi et al., 2008). They enhance targeted delivery, reduce waste, and lower environmental impacts. Nanoparticles can be used via foliar application on plants, seed treatments, and soil amendments with other fertilizers (González-Melendi et al., 2008; Shelar et al., 2023; Takeshita et al., 2023).

In this study, Fe and Zn NPs were synthesized using PGPR and then characterized to ensure uniformity, polarity, morphology, crystallinity, and compatibility. The impact of NP delivery methods was assessed on the growth and nutritional content of wheat (WH 1105). Furthermore, the mechanism of the microbe–NP interaction was studied via growth kinetics, bacterial activity, and production of metabolites.

A broad array of bacterial metallic NPs has been used in the agriculture sector. These include oxide nanoparticles of gold (Tikariha et al., 2017), cobalt (Eltarahony et al., 2018), silver (Gopinath et al., 2017), copper, zinc (Zaki et al., 2021), titanium (Kumaravel et al., 2021), and iron (Crespo et al., 2017). Bacterial isolates from maize roots were screened based on their plant growth-promoting (PGP) traits, and five bacterial isolates were used for maize growth enhancement (Prischl et al., 2012). Similarly, Maheshwari et al. (2022) isolated 355 bacteria from the root and nodules of *Pisum sativum* and *Cicer arietinum* and checked their effect on the leguminous plant growth and development, taking 25 selected isolates. The selection of bacteria based on PGP traits is crucial as it indicates their significant potential to enhance plant

growth. This study reports the application of bacteria having plant growth-promoting abilities for the synthesis of FeNPs and ZnNPs and evaluates their effect in combination with bacteria on wheat growth and nutritional content. This could be a sustainable approach in nanotechnology via enhancing the efficacy of existing PGPR toward the biofortification of agricultural products and alternatives to agrochemicals.

2 Materials and methods

2.1 Bacterial isolation and its tolerance toward Fe and Zn

2.1.1 Bacterial isolates

A total of 10 bacteria (SL1–SL10) were isolated from wastewater treatment, slug (site), and slag (site) Fe-enriched sites from Hisar (Haryana, India) using a serial dilution method (Rana et al., 2011). Soil samples were diluted up to 10^{-8} with sterilized water, and 100 µL from final dilutions was spread on Luria Bertani (LB) agar plates, followed by overnight incubation at 28 ± 2°C. The bacteria were isolated on the basis of distinguished colony shape, pigmentation, and other morphological features. Furthermore, six plant growth-promoting isolates (RP24, TMG3, WF, WH, WD, and AW5) were obtained from the Microbial Genomics Laboratory (115A), Department of Microbiology, College of Basic Sciences and Humanities, Chaudhary Charan Singh Haryana Agricultural University, Hisar, Haryana (India). The bacteria were grown on an LB agar medium and stored at 4°C for further use.

2.1.2 Salt tolerance of bacterial isolates

The isolates were evaluated for their Fe and Zn tolerance on nutrient agar media supplemented with different concentrations of ferric chloride ($FeCl_3$) and zinc sulfate ($ZnSO_4$) (3 mM, 6 mM, 9 mM, and 12 mM). The iron and zinc solutions were added to the growth media via syringe filtration before being poured onto a Petri plate. The bacteria were grown on the prepared media at 28 ± 2°C, and colony growth diameter was observed after 48 h of incubation.

2.2 Plant growth-promoting (PGP) traits of bacteria

The selected four bacterial isolates (AW5, WH, SL5, and SL9) were screened for a wide array of PGP traits. Phosphate solubilization was analyzed using Pikovskaya medium (Hi Media). The bacteria were grown in LB medium (12 h at 28 ± 2°C). The grown bacterial cell culture (10 µL) was spotted on solid medium and also inoculated in liquid Pikovskaya medium to estimate the phosphate solubilization activity via observing a clear zone around the spot on the solid medium. For the liquid assay, bacteria were grown for 5 days, followed by analysis using a molybdenum blue colorimetric assay to measure solubilized phosphate (Pikovskaya, 1948).

Zinc solubilization estimation was performed by supplementing 1% zinc sulfate in LB medium, and the zone was measured for zinc solubilization on the solid medium as performed for phosphate solubilization. The zinc quantification in liquid medium was performed by growing bacteria for 4–5 days, followed by zinc analysis using Atomic Absorption Spectroscopy (AAS) (Di Simine et al., 1998).

The Salkowski colorimetric method was used to detect the production of indole-3-acetic acid (IAA) by growing bacteria in yeast extract mannitol broth supplemented with 100 µL/mL concentration of tryptophan for 3–7 days at 28 ± 2°C. A pink/red color formation through the mixing of Salkowski reagent solution indicated the formation of IAA, followed by analysis using a spectrophotometer (530 nm) (Tang and Bonner, 1948; Rana et al., 2011; Kumar et al., 2022). Siderophore production was detected using Chrome Azurol S dye in an agar plate with a modified method (Schwyn and Neilands, 1987). The bacterium was grown on CAS agar medium, and a zone was observed with yellow pigmentation by chelating iron from the CAS dye for siderophore-producing bacteria.

2.3 Bacterial synthesis of Fe and Zn nanoparticles

The four selected bacterial isolates (AW5, WH, SL5, and SL9) were grown in Luria Bertani (LB) broth in an incubator shaker (150 rpm, 5 days, 28 ± 2°C). The bacterial cells were harvested through centrifugation (6,000 rpm, 10 min), and the supernatant was collected. The supernatant was mixed with $FeCl_3$ (1mM) or $ZnSO_4$ (1mM) in a 1:1 ratio and mixed via stirring at 800 rpm (at 50°C for 3 h) and kept overnight for shaking at 150 rpm (28 ± 2°C). The mixture was centrifuged (8,000 rpm, 10 min), followed by washing (three times) with sterile distilled water. Following washing with ethanol (70%), nanoparticles were dried at 50°C. LB broth without bacterial growth was used as a control by following the mixing of $FeCl_3$ or $ZnSO_4$ under the same conditions as described above. The following synthesis methods were adopted with modifications (El-Naggar and Abdelwahed, 2014; Omajali et al., 2015; Majeed et al., 2021).

2.4 Characterization of Fe and Zn nanoparticles

The size, morphology, surface functionality, elemental composition, and crystallinity of the synthesized FeNPs and ZnNPs were studied using particle size analysis (PSA), zeta potential analysis, scanning electron microscopy (SEM), energy dispersive X-ray spectroscopy (EDX), X-ray diffraction (XRD), and Fourier transform infrared spectroscopy (FTIR). FTIR analysis was performed using a PerkinElmer Spectrometer Spectrum 3 (USA) to study the surface chemistry of FeNPs and ZnNPs. The dried NPs were analyzed using the KBr pellet method in the range of 400–4,000 cm^{-1}. The particle size and zeta potential of the nanoparticles were assessed using dynamic light scattering (DLS) techniques (Malvern Panalytical Zeta Sizer Pro). A fixed concentration (1 mg/mL) of NPs was suspended in distilled water and sonicated (30 min) with a probe sonicator (SONICS) prior to analysis in a polystyrene cuvette. The morphology of the synthesized NPs was examined using field emission scanning electron microscopy (FESEM; JEOL, version 2). The FeNPs and

ZnNPs were immobilized onto a conductive sticky carbon disk, followed by gold coating to enhance the conductivity of the specimens. The coating thickness was carefully controlled (~ 10 nm) to ensure adequate conductivity while allowing detailed surface observation. The elemental composition of the FeNPs and ZnNPs was analyzed using EDX coupled with the FESEM (JEOL, version 2). The crystallinity of FeNPs and ZnNPs was investigated using a powder X-ray diffractometer. This analysis helped get the average dimensions of the scattering regions within the NPs and enabled the accurate identification of crystalline phases. Annealing of amorphous BioNPs was done by keeping them in a tubular furnace at 500°C (2 h) under a nitrogen environment. Furthermore, the annealed NPs were characterized using pXRD (Nandhini et al., 2019; Majeed et al., 2021; Mathur et al., 2021).

2.5 Effect of Fe and Zn nanoparticles on bacterial growth and PGP traits

The bacterial isolate AW5 was grown in LB broth supplemented with biosynthesized Fe and Zn amorphous nanoparticles individually at different concentrations (1 ppm, 5 ppm, 10 ppm, 20 ppm, 30 ppm, 40 ppm, and 50 ppm) to check the effect of NPs on bacterial growth. The growth of bacteria was measured at OD_{600} nm after 12 h and 24 h. The optimized concentration, which shows a significant effect on bacterial growth enhancement, was compared with standard chemically synthesized (Sigma Aldrich Chemicals Pvt. Ltd.) and crystalline (after annealing of biologically synthesized NPs) Fe and Zn NPs. The effect of the optimized dose of NPs was checked on PGP traits of AW5, namely, IAA production, siderophore production (Butaite et al., 2017; Maheshwari et al., 2019; Payne, 1994; Shang et al., 2019), and zinc and phosphate solubilization, by following quantitative assays using modified methods (Rana et al., 2011; Bhutani et al., 2021).

2.6 Evaluation of the combined effect of NPs and bacteria on wheat growth and nutritional value

The optimized concentrations of Fe and Zn NPs that enhanced microbial growth under *in vitro* study were applied in combination with bacteria for the treatment of wheat seeds.

2.6.1 Pot experiment

The effects of synthesized Fe and Zn NPs, individually as well as in combination with PGPR (AW5), were tested on wheat. Wheat seeds were primed with the suspension of NPs and bacterial culture before sowing. The optimized doses of Fe and Zn NPs, which showed enhanced effects on the growth bacteria and PGP traits, were selected to evaluate their effect on growth, yield, and nutritional content of wheat under pot house conditions. A total of 18 treatments were designed, and the recommended dose of fertilizer (RDF) N120P60K60 was added in all the treatments, except the absolute control following two split doses of nitrogen as follows: T1: Absolute control; T2: RDF control; T3: RDF + PGPR; T4: RDF + PGPR + FeNPs (20 ppm); T5: RDF + PGPR + FeNPs (100 ppm); T6: RDF + PGPR + ZnNPs (20 ppm); T7: RDF + PGPR + ZnNPs (100 ppm); T8: RDF + PGPR + ZnNPs and FeNPs (20 ppm); T9: RDF + PGPR + ZnNPs and FeNPs (100 ppm); T10: RDF + PGPR + Foliar treatment ($FeCl_3$), T11: RDF + PGPR + Foliar treatment ($ZnSO_4$); T12: RDF + PGPR + $ZnSO_4$ and $FeCl_3$, T13: RDF + PGPR + Foliar treatment (FeNPs-20 ppm); T14: RDF + PGPR + Foliar treatment (FeNPs-100 ppm); T15: RDF + PGPR + Foliar treatment (ZnNPs-20 ppm); T16: RDF + PGPR + Foliar treatment (ZnNPs-100 ppm); T17: RDF + PGPR + Foliar treatment (ZnNPs and FeNPs-20 ppm); T18: RDF + PGPR + Foliar treatment (ZnNPs and FeNPs-100 ppm).

2.6.2 Seed priming

Surface sterilization of wheat seeds was performed with sodium hypochlorite (4%), followed by washing with sterilized distilled water (DW) and drying. The sterilized seeds were primed with FeNPs (20 ppm, 100 ppm) or ZnNPs (20 ppm, 100 ppm) or a combination of both nanoparticles (20 ppm; 100 ppm), followed by PGPR or combination (PGPR and NPs) for a 1-h treatment. The nanoparticle stock (1,000 ppm) was prepared by dispersing it in double-distilled water by sonication. Working concentrations (20 ppm and 100 ppm) were prepared by dilution of stock solution and employed for seed priming and foliar application. A foliar spray was performed on the crop at the three-leaf stage and the milking head stage.

2.6.3 Soil microbial enzymatic activity and plant biochemical analysis

The soil mix (5 g) with solution A (3% TTC (2,3,5 triphenyl tetrazolium chloride) and distilled water 1:2) was used to determine the dehydrogenase activity. Samples were incubated at 37°C for 24 h (in dark) after vigorous mixing. After incubation, methanol (10 mL) was added to the reaction and filtered (Whatman No. 1 paper). The absorbance of the filtrate was recorded at 485 nm using a spectrophotometer with methanol as a blank (Thalmann, 1968). The potassium phosphate buffer (5 mL, pH 7.6, 60 mM) was mixed with soil (1 g), followed by the addition of fluorescein diacetate (FDA) solution (10 µL) and incubation (37°C, 1 h). After incubation, acetone (200 µL, 5% v/v) was added to stop the reaction and filtered. The absorbance was recorded at 485 nm using a spectrophotometer method (Green et al., 2006).

After harvesting the crop, different parameters like auxin (Manna et al., 2024) and chlorophyll content (Wellburn, 1994) were analyzed. Fresh plant tissues were weighed 0.1 gm and crushed after freezing in deep at −20°C for 2 h. An aliquot of ethanol (~2 mL) was added to the powdered sample before thawing, followed by thorough grinding. The homogenate (1 mL) was transferred to an Eppendorf tube and centrifuged at 10,000 × g for 2 min at 4°C. The supernatant (100 µL) was mixed with 900 µL of the reagent (mixture of water: concentrated sulfuric acid: 0.5 M $FeCl_3$ (25:15:0.75) and incubated at room temperature for 30 min. Absorbance was recorded at 540 nm, and the auxin concentration was calculated using a standard curve (Manna et al., 2024). The chlorophyll content was analyzed following the modified method of Wellburn (1994). Fresh tissue (0.1 g) was crushed using a chilled mortar and pestle, followed by the addition of methanol (5 mL). The homogenate was incubated at 65°C for 30 min in the dark. The mixture was centrifuged at 10,000 × g for 10 min, and the supernatant was analyzed using a spectrophotometer at 666 nm and 653 nm

wavelengths. Total chlorophyll content, chlorophyll a, and chlorophyll b were calculated using the following equations: Chlorophyll a (μg/g) = (15.65 × A666–7.34 × A653) × 50; chlorophyll b (μg/g) = (27.05 × A653–11.21 × A666) × 50 (Wellburn, 1994).

2.6.4 Plant physiological parameters

The pots were filled with water overnight before harvesting the plants with their roots intact. The plant roots were washed to remove excess soil and dried before measuring biomass and shoot and root length (cm). Plant biomass (g) was measured with spikes, followed by grain harvesting and grain weight (100 seeds per treatment). All experiments were performed in triplicate, and the average was reported.

2.6.5 Nutrient analysis

The plant samples were prepared using a standard protocol. In brief, plant straw and grain fine powder (0.5 g) were added with diacid (HNO_3+$HClO_4$, 4:1, 10 mL) and heated until a clear, colorless solution (reduced up to 3–4 mL) was obtained. The solution was cooled, filtered, and transferred to a volumetric flask, followed by analysis (Huang et al., 2004). In the case of P, the analysis digested plant material (1–5 mL) was taken in a volumetric flask, followed by the addition of 2,4 di-nitrophenol indicator (2–3 drops). Ammonia solution was added until a yellow color appeared. Furthermore, HCl (6 N) was drop-wise added up to a colorless appearance, followed by the addition of the vanadomolybdate solution (5 mL) and diluted up to 25 mL with distilled water, mixed well, and analyzed using a spectrophotometer (440 nm wavelength). The soil sample (2.0 g) was taken in a glass bottle (100 mL), to which was added a pinch of activated charcoal (Darco G-60). Sodium bicarbonate ($NaHCO_3$) solution (40 mL of 0.5 M) was added to the soil sample, agitated for 30 min, and filtered for analysis of nutrients (Alban and Kellogg, 1959).

2.6.5.1 Analysis of phosphorus in soil and plant

The soil filtrate was transferred to a volumetric flask, followed by the addition of ammonium molybdate solution (5 mL), and gently agitated to flush out CO_2. Furthermore, distilled water was slowly added to make up the volume (20 mL), 1.0 mL of freshly prepared tin chloride ($SnCl_2$) solution was added, and the volume was made up with double-distilled water (DDW), followed by analysis (at 660 nm) using a spectrophotometer.

2.6.5.2 Analysis of potassium in soil, plant, and grain

The samples for soil (5.0 g) and plants/grains (0.5 g) were transferred to a conical flask (100 mL), followed by the addition of NH_4OAc solution (25 mL), mixed well, and filtered for analysis. The analysis of K in the digested samples was performed using a flame photometer.

2.6.5.3 Analysis of iron, zinc, manganese, and copper

The digested and extracted samples discussed above were used for micronutrient analysis using Atomic Absorption Spectroscopy (AAS) with reference standards of Fe, Zn, Mn, and Cu.

2.6.6 Proximate analysis of wheat grains

Proximate analysis of wheat grain was performed using standard laboratory protocols. Moisture content in wheat grain samples (5 g, dried for 15 min, 100°C) was estimated. The moisture content was calculated using the following formula: Moisture (%) = (W2/W1) × 100, where W1 is the initial weight of the sample (g), and W2 is the weight loss (g) after drying. To determine the ash content, a grain sample (5.0 g) was placed in a silica crucible and heated in a muffle furnace (550°C, 15 min). The crucible was then removed, cooled in a desiccator for 1 hour, and weighed. The sample was heated on a hot plate until smoking ceased and thoroughly charred until it became white. The ash content was calculated using the formula: Ash (%) = (W2/W1) × 100, where W1 and W2 are the weight of the sample (g) and the loss of weight (g) in the sample after drying, respectively.

To determine the crude fat content, a finely ground wheat grain sample (5.0 g) was placed in an extraction thimble. The thimble was placed in an extractor and connected to a weighed flask containing petroleum ether (100 mL). The extractor was connected to a reflux condenser, and the sample was extracted under reflux for 2 h. After extraction, the petroleum ether extract was evaporated to dryness, and 2 mL of acetone was added. Air was gently blown into the flask to remove the last traces of the solvent. The flask containing the fat residue was dried in a hot air oven (100°C, 10–15 min), then cooled in a desiccator, and weighed. The crude fat content was calculated using the formula: Crude Fat (%) = ((W3 − W2)/ W1) × 100, where W1 is the weight of the sample before drying (g), W2 is the weight of the empty flask (g), and W3 is the weight of the flask with the fat residue (g).

2.6.6.1 Crude fiber (%)

To determine crude fiber content, a fat-free dried wheat grain sample (1–2 g) was placed in a beaker containing H_2SO_4 (200 mL of 1.25%), followed by the addition of a few drops of antifoam. The mixture was heated to boil (1 min) using a crude fiber apparatus and kept for boiling (30 min) with intermittent stirring. The content was filtered and washed with 200 mL of sodium hydroxide (1.25%). The solution was boiled for 30 min, and the insoluble matter was transferred to a sintered crucible and washed using boiling water until acid-free, followed by washing with alcohol and acetone. The sample was then dried at 100°C to constant weight and converted to ash in a muffle furnace at 550°C for 1 h, followed by cooling in a desiccator and weighing. The crude fiber content was calculated using the formula: Crude fiber (%) = ((W2 − W3)/W1) × 100, where W1 is the weight of the sample (g), W2 is the weight of the insoluble matter (g) (weight of crucible + insoluble matter − the weight of crucible), and W3 is the weight of the ash (g) (weight of crucible + ash).

2.6.6.2 Carbohydrate (%)

Carbohydrate was calculated by subtracting the sum of the other proximate components (crude protein, crude fat, crude fiber ash, and moisture) from 100.

2.7 Statistical analysis

All experiments were performed in triplicate and expressed as mean values and standard deviations (mean ± SD). One-way analysis of variance (ANOVA) was conducted at a 95% confidence level ($p < 0.05$). The Tukey's honestly significant

difference (HSD) test was performed for multiple comparisons to determine statistically significant differences and represented with different alphabets in figures. For graphical representation and data visualization, OriginPro 2024b (OriginLab Corporation, USA) and SigmaPlot version 11.0 (Systat Software Inc., USA) were utilized to construct charts and figures.

3 Results and discussion

3.1 Fe and Zn tolerance of bacterial isolates

The bacterial isolates (SL5, AW5, and WH) were tolerant to iron ($FeCl_3$) up to 9 mM on growth media. Isolates RP24, TMG3, WD, and WF were tolerant up to 6 mM, while other isolates showed no tolerance to $FeCl_3$-containing media (Supplementary Figure S1). The isolates, namely SL5, SL9, AW5, and WH, were tolerant up to 9 mM on growth media containing zinc ($ZnSO_4$). Other isolates showed tolerance up to 6 mM against $ZnSO_4$-supplemented growth media, except TMG3, SL6, and SL7, which showed zero tolerance or up to 3 mM only.

3.2 PGP traits of selected bacterial isolates

Bacterial isolates (AW5, WH, SL5, and SL9) having maximum tolerance to $FeCl_3$ or $ZnSO_4$ salts were tested for PGP traits (IAA and siderophore production, zinc and phosphate solubilization). AW5 produced maximum IAA (10.5 µg/mL) and showed the highest solubilization index of iron (1.3), zinc (2.0), and phosphate (2.0). WH, SL5, and SL9 showed IAA production up to 7.5 µg/mL, 1.5 µg/mL, and 5.0 µg/mL, respectively. Moreover, the iron solubilizing index of WH was 1.5 (Figure 1). The bacteria having the ability to produce these traits have been successfully used to increase crop productivity and biofortification in a sustainable manner (Rana et al., 2011; Rana et al., 2012; Guardiola-Márquez et al., 2023).

3.3 Synthesis of nanoparticles

FeNPs and ZnNPs were synthesized using bacterial isolates AW5, WH, SL5, and SL9. The hydrodynamic diameters (nm) of synthesized bacterial (amorphous) nanoparticles (Fe, Zn) were (135, 197), (572, 471), (411, 524), and (468, 430), respectively. AW5-mediated FeNPs and ZnNPs were the smallest, showed PGP traits, and were therefore selected for further synthesis and application (Supplementary Table S1; Supplementary Figure S2). There are a number of studies where bacteria have been used for NP synthesis, for example, *Bacillus licheniformis*, *Alishewanella* sp. WH16-1, and *Mycobacterium* sp. MRS-1 were employed for the synthesis of Au, Se, and Co_3O_4 NPs, respectively (50–220 nm) using inorganic salts (Tikariha et al., 2017; Xia et al., 2018; Sundararaju et al., 2020).

3.4 Characterization of FeNPs and ZnNPs

The standard Fe and Zn oxide nanoparticles were used as reference material with bacterial (amorphous and annealed) NPs. Sharp peaks in pXRD patterns indicate purity and well-defined crystal structure of standard nanoparticles (Figures 2A,B). The amorphous nature of synthesized nanoparticles was confirmed by no discernible peaks. However, after annealing, distinct peaks emerged, possibly due to the crystallization of bacterial nanoparticles (Figures 2C,D). This underscores the influence of experimental conditions on the nucleation and growth of crystals, elucidating the dynamic nature of nanoparticle formation.

The diffractogram of standard FeNPs closely matches with an inverse spinel structure with corresponding peaks (2θ) at 31.64°, 36.29°, 47.75°, and 69.23° and Miller indices that correlate to the plane (220), (311), (511), and (440) (Figure 2A). The pXRD patterns of standard ZnNPs show noticeable peaks (2θ), 31.64°, 34.43°, 36.29°, 47.75°, 56.51°, 62.90°, 67.98°, and 69.23° with corresponding Miller indices to the planes (100), (002), (101), (102), (110), (103), (112), and (201), closely matching with the wurtzite structure (Figure 2B). After annealing, the diffractogram of bacterial FeNPs displays an inverse spinel structure with peaks (2θ) at 31.64°, 36.29°, 47.75°, and 69.23°, corresponding to Miller indices of the plane (220), (311), (511), and (440) (Figure 2C). Similarly, annealed ZnNPs exhibited peaks (2θ) at 31.64°, 34.43°, 36.29°, 47.75°, 56.51°, 62.90°, 67.98°, and 69.23°, corresponding to plane (100), (002), (101), (102), (110), (103), (112), and (201), confirming the wurtzite structure (Figure 2D).

The sharp and narrow peaks in p-XRD patterns of standard NPs exhibit their purity and well-defined crystal structure. The X-ray diffraction analysis revealed no peaks for bacterial NPs because they exist as an amorphous material. Several research studies indicate that biological Fe and Zn NPs have an amorphous structure (Kouhbanani et al., 2019; Menazea et al., 2021). Amorphous NPs exhibit liquid-like properties at the molecular level and solid-like properties at the macroscopic level. Annealing of amorphous nanoparticles was performed to prepare the crystalline phase and its effect on biological activity. However, the biological activity of annealed bacterial NPs was reduced. The crystallinity enhancement in reports has also been observed with increased temperature (400°C–600°C) (Dehkordi et al., 2015; Farahmandjou and Soflaee, 2015; He et al., 2019). The bacterial FeNPs and ZnNPs after annealing exhibited inverse spinel and wurtzite structures, respectively, similar to the available reports (Kalpana et al., 2018; Shukla et al., 2015)). The surface morphology of amorphous NPs was smooth, and that of annealed NPs was similar to standard FeNPs and ZnNPs in terms of average size. The size of the Fe and ZnNPs (50–200 nm) varied, and a flaky structure was observed for both.

The presence of functional groups on standard and bacterial NPs was investigated using Fourier transform infrared spectroscopy (FTIR). The peaks at 550–600 cm^{-1}, 1,096 cm^{-1}, 1,644–1,651 cm^{-1}, and 3,350–3,401 cm^{-1} correspond to the functionalities Fe-O, C-O, C=C, and O-H, respectively, both in standard and bacterial FeNPs (Figure 3A). The lower wavenumber observed for bacterial NPs may be attributed to organic compound capping. The broad band corresponding to the stretching vibration of the hydroxyl peak is associated with polyphenols or flavonoids, which act as reducing and stabilizing agents. Peaks of C-O, C=C denote the existence of a

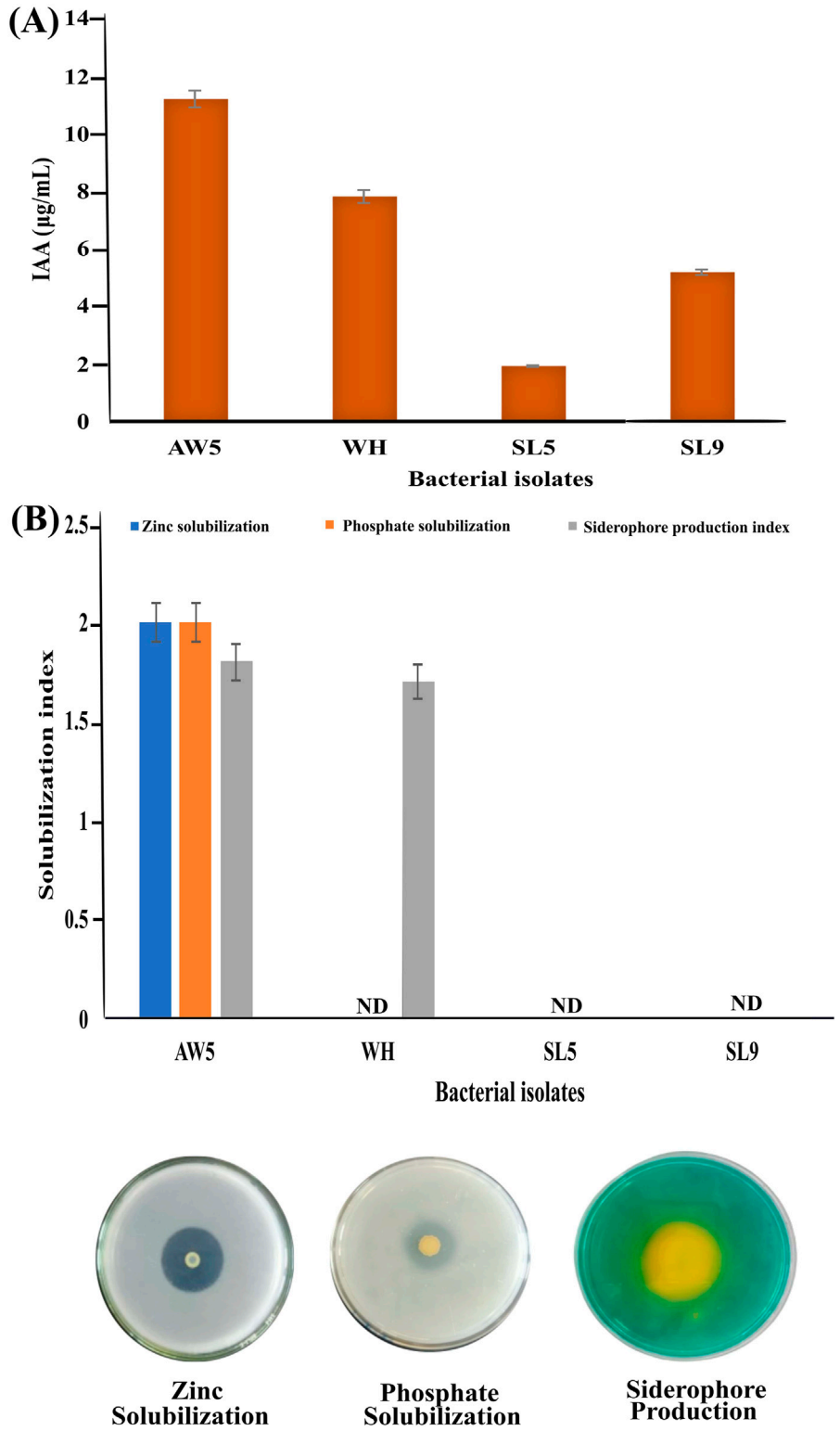

FIGURE 1
Plant growth-promoting traits of bacterial isolates (AW5, WH, SL5, and SL9) **(A)** Indole-3-acetic acid production and **(B)** Zinc and phosphate solubilization index and siderophore production index.

carbohydrate ring of polysaccharides from bacterial metabolites. Similarly, peaks at 560–580 cm^{-1}, 1,040–1,050 cm^{-1}, 2,880–2,900 cm^{-1}, and 3,350–3,501 cm^{-1} correspond to Zn-O, Zn-OH, C=O, -CH_2-CH_3, and O-H, respectively, in bacterial and standard ZnNPs (Figure 3B). Peaks corresponding to hydroxyl groups of alcohols or phenolics in standard NPs are broader and

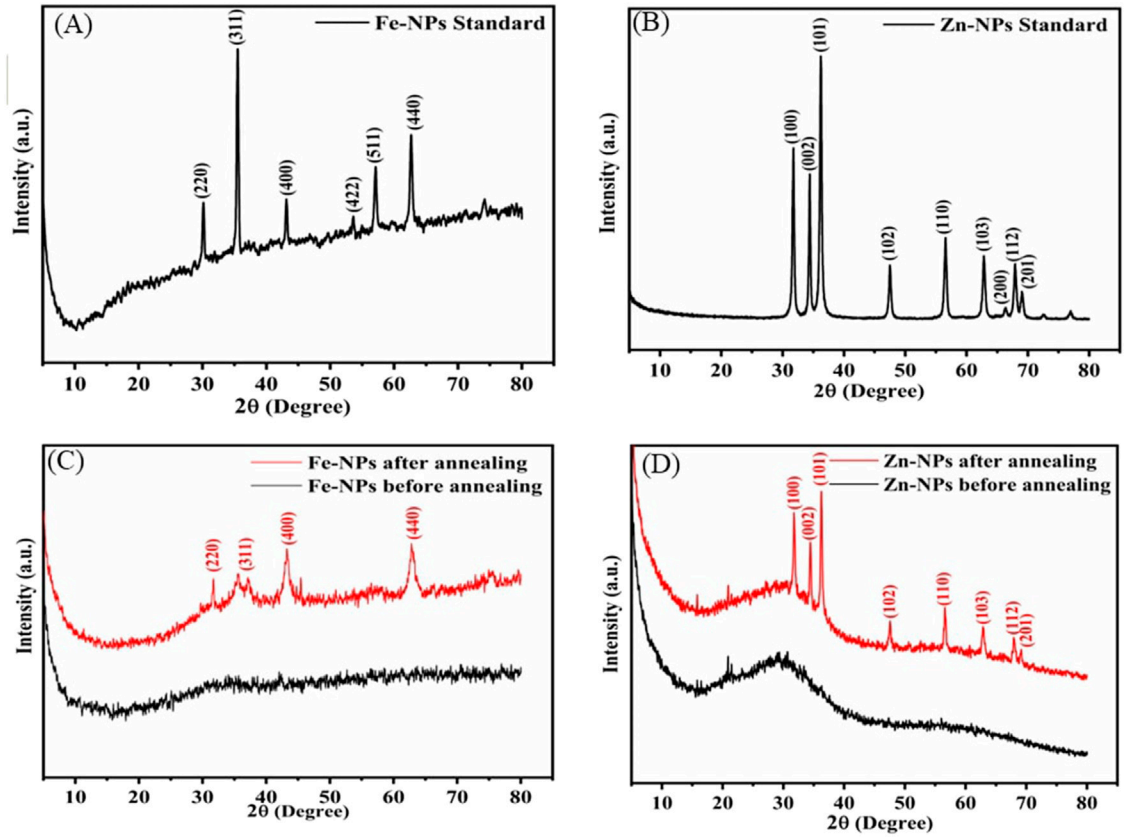

FIGURE 2
The diffractogram of standard FeNPs **(A)**, standard ZnNPs **(B)**, bacterial FeNPs **(C)**, and ZnNPs **(D)**.

shifted in bacterial ZnNPs, validating the biochemical involvement. Bands corresponding to–CH_2 and–CH_3 stretching vibrations suggest the presence of fatty acids or proteins with organic molecule capping, which may improve colloidal stability in biological nanoparticles. The slight downshift of Zn-O in biologically synthesized ZnNPs may be attributed to organic capping agents, typically contributed by bacterial metabolites. The FTIR spectra of FeNPs and ZnNPs distinctly validate the presence of metal–oxygen bonds (Fe–O and Zn–O), showing successful nanoparticle synthesis. The biological pathways have extra and slightly shifted peaks corresponding to hydroxyl, carbonyl, alkene, and aliphatic groups that are not present or less intense in standard nanoparticle counterparts. These additional peaks suggest the occurrence of bioorganic molecules like phenolics, proteins, flavonoids, or polysaccharides, which serve as significant reducing, capping, and stabilizing agents in green synthesis. Thus, enhanced biocompatibility and functionality may be the result of nanoparticle functionalization in biological synthesis pathways, as demonstrated by FTIR analysis.

The morphology, shape, and size of standard and bacterial FeNPs and ZnNPs were analyzed using SEM. The shape of the particles was spherical and highly agglomerated. The size of standard FeNPs and ZnNPs was 50–200 nm and <100 nm, respectively. After annealing, the size of bacterial Fe and ZnNPs was 50–150 nm and <100 nm, respectively. However, before annealing, the bacterial (amorphous) NPs (100–200 nm) showed agglomeration due to their amorphous nature (Figure 4). Energy-dispersive X-ray analysis (EDX) revealed that standard FeNPs contained 74.1% Fe and 25.9% oxygen, while standard ZnNPs contained 73.1% Zn and 26.9% oxygen. Before annealing, bacterial (amorphous) FeNPs contained 56.4% Fe, 42.4% oxygen, and traces of Ti and S. Bacterial ZnNPs had 43.5% Zn, 30.3% oxygen, and traces of C and P. After annealing, bacterial FeNPs showed 68.1% Fe and 31.4% oxygen; ZnNPs had 65.9% Zn and 34.1% oxygen (Supplementary Figure S3). The research on nanoparticle dimension provides information about the effect of types and size of NPs and their formulations on plant–microbe interaction, nutrient dynamics, and modulation on their biological activity (Kumar et al., 2025). The charges on bacterial FeNPs (−45.21 mV) and ZnNPs (−25 mV) provide stability for better plant uptake and make them suitable to be used as a biostimulant. NPs get colloidal stability due to strong inter-particle repulsion and moderate negative zeta potential. The stable NPs in colloidal form interact effectively with plants for extended periods.

3.5 Effect of Fe and Zn NPs on bacterial growth and their PGP traits

The synthesized NPs were tested to optimize their dose on bacterial growth in a liquid medium and analyzed their effect on plant growth-promoting traits of bacteria.

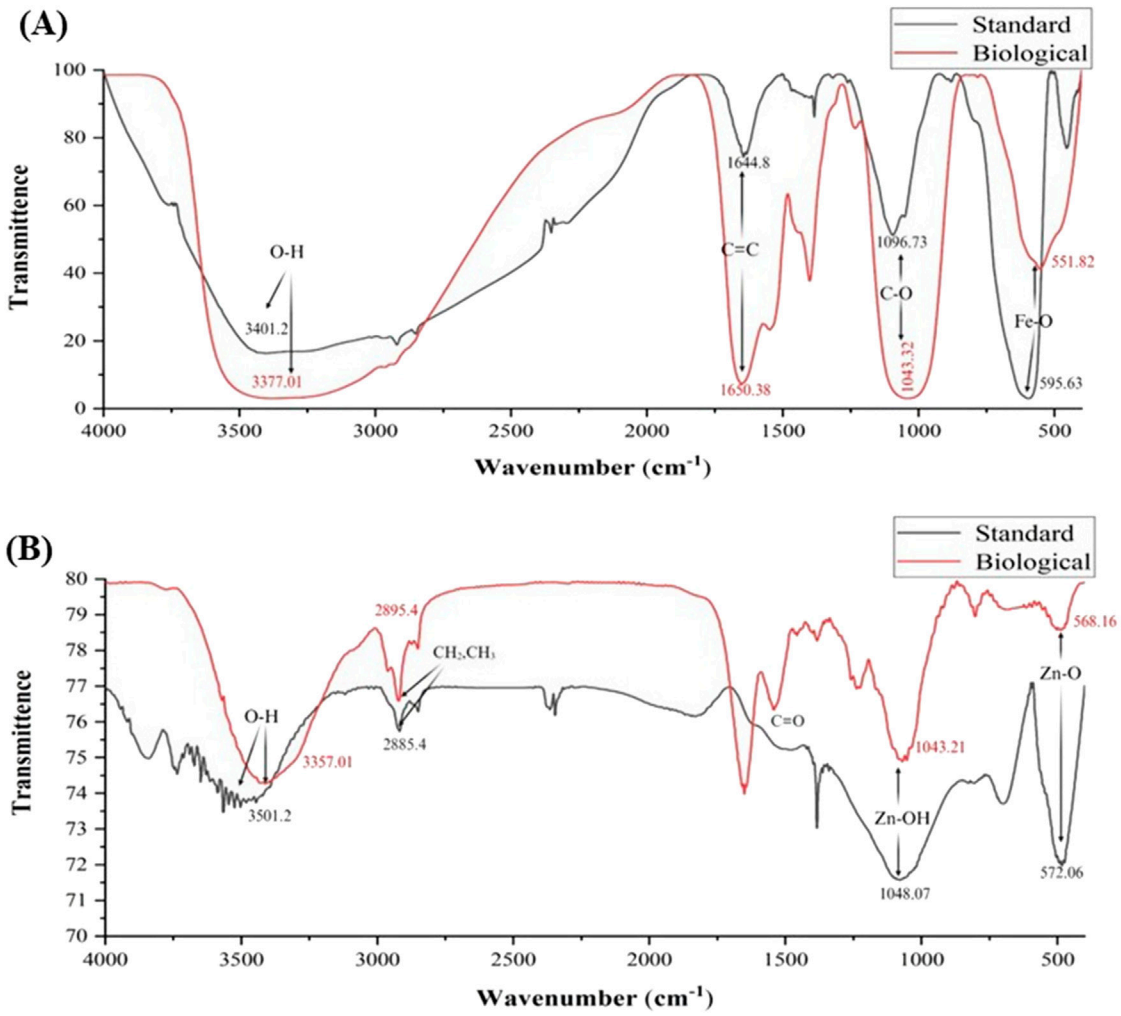

FIGURE 3
Surface chemistry of standard and bacterial (AW5) FeNPs **(A)** and ZnNPs **(B)**.

3.5.1 Effect on the growth profile

The impact of amorphous Fe and Zn NPs on the growth of AW5 in a liquid medium was dependent on the concentration (1 ppm, 5 ppm, 10 ppm, 20 ppm, 30 ppm, 40 ppm, and 50 ppm). The maximum growth of AW5 was observed at 20 ppm for Fe (2.3×10^8 CFU/mL) and Zn (2.1×10^8 CFU/mL), with an increase in bacterial growth (up to 19%) versus control without NPs (Figures 5A,B). The effect of standard and annealed Fe and Zn NPs on the growth of bacteria was compared with their amorphous form in a liquid medium at an optimized concentration (20 ppm) of NPs. The amorphous bacterial nanoparticles (BNPs) significantly increased bacterial count with the amendment of Fe (12%–18%) and Zn (15%–17%) versus standard NPs and crystalline (annealed) BNPs, respectively. However, the standard (S) and annealed (A) nanoparticles did not show any significant effect on bacterial growth enhancement (Figure 6). The positive impact of amorphous Fe and Zn nanoparticles on bacterial growth showed their better compatibility and employability in sustainable agriculture.

3.5.2 Effect of nanoparticles on PGP traits of bacteria

The effect of amorphous FeNPs and ZnNPs on the PGP traits of AW5 was checked with optimized doses of NPs (10 ppm, 20 ppm, and 30 ppm) supplemented with a liquid medium. The NP treatment enhanced IAA production significantly (up to 39%) with ZnNPs (20 ppm) versus control (without NPs). However, IAA production in the case of FeNP treatment was not significant. Phosphate and zinc solubilization were increased in the case of FeNPs (60%) and ZnNPs (35%) with a 20 ppm dose. Moreover, siderophore production significantly improved by up to 10% with FeNPs (20 ppm) (Figure 7).

The enhanced growth and PGP traits of AW5 in response to NPs indicate the improved dynamics of nutrients leading to the enhancement of biochemical activity in bacteria for soil health and plant growth promotion. In this study, we have observed for the very first time the effect of bacterial Fe and Zn NPs on the PGP traits of rhizobacteria. It is pertinent to mention that the studies have generally reported the toxicity of NPs towards bacteria. For example, Chatterjee et al. (2011) reported a declined effect of different

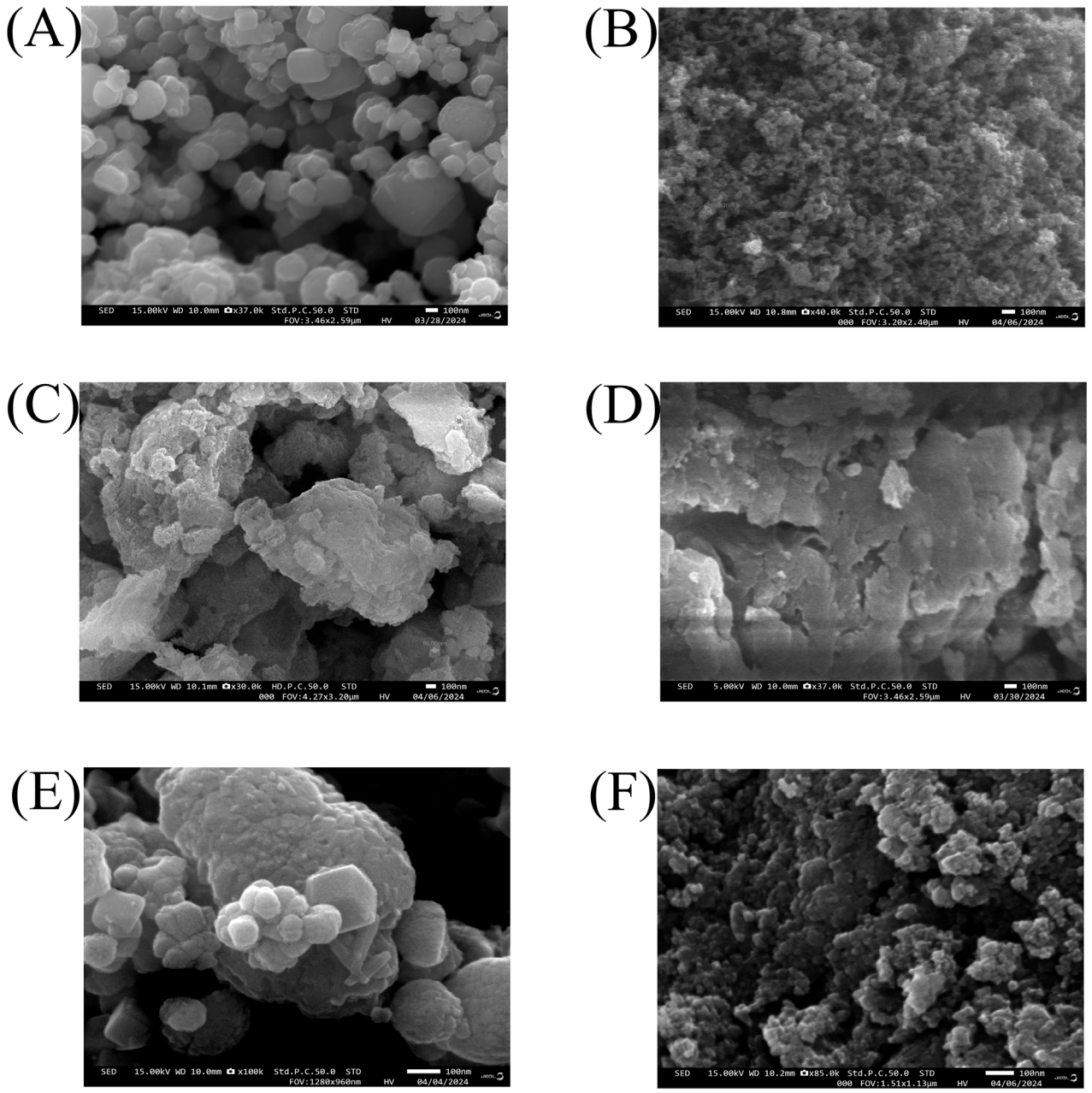

FIGURE 4
Morphology of standard FeNPs and ZnNPs **(A,B)** before annealing **(C,D)** and after annealing **(E,F)**, respectively.

concentrations (50–200 µg/mL) of chemically synthesized iron oxide NPs on the growth of *Escherichia coli* at 6-h incubation due to reactive oxygen species (ROS) superoxide, hydroxide radical, and singlet oxygen (Chatterjee et al., 2011). Chemically synthesized FeNPs (10–100 ppm) showed a negative effect on the *Serratia* growth and reduced production of biosurfactants, while a positive effect of bacterial NPs on the growth of PGPR and activity thereof was noticed in our study within the same concentration range. Similar to our study, Kaur et al. (2024) reported an enhanced effect of titanium NPs (20 ppm) on the PGP traits of *Rhizobium*, namely, IAA, siderophore production, and phosphate solubilization.

3.6 Combined effect of NPs and bacteria on wheat growth and nutritional value

Bacterial FeNPs and ZnNPs have an advantage over chemical NPs, acting as biocompatible nutrient sources for bacterial growth. The improved PGP characteristics, including IAA production together with phosphate solubilization mechanisms, allowed plants to develop stronger roots, which enhanced their ability to acquire nutrients that led to increased wheat biofortification and yield. The effects of NPs and bacteria were analyzed by observing plant growth attributes and other nutritional parameters as described below.

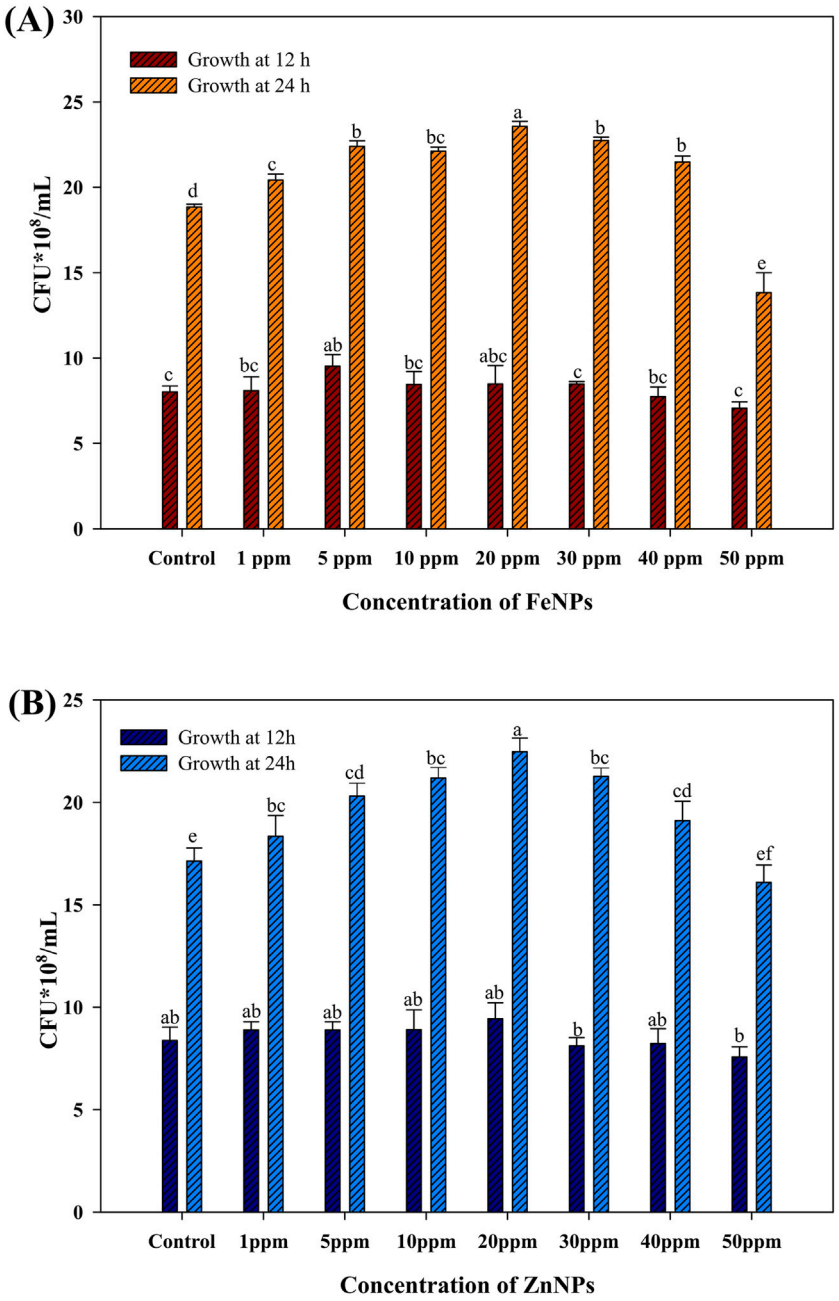

FIGURE 5
Effect of bacterial Fe and Zn nanoparticles (amorphous) on AW5 growth at different concentrations (ppm) **(A)** FeNPs; **(B)** ZnNPs. Error bars represent standard deviation, and different letters on the bar show significant differences ($p < 0.05$, $n = 3$).

3.6.1 Soil microbial enzymatic activity

The effect of NPs on soil enzymes (dehydrogenase and fluorescein diacetate) was studied. The FDA activity ranged from 11.43 to 20.4 µg fluorescein/g soil/h. Foliar applications of ZnNPs (100 ppm) with RDF and PGPR showed a maximum increase (64%) in T16 versus the RDF control (T2). It was up to a 53% increase compared to other treatments containing NPs (Figure 8A). The dehydrogenase activity ranges from 1.49 µgTPF/g soil/d to 2.2 µgTPF/g soil/d. The maximum increase (53%) was observed in T7 (seed-primed with RDF + PGPR+ ZnNPs, 100 ppm) versus the RDF control (T2). Moreover, dehydrogenase activity was also increased in other NP treatments up to 42% (Figure 8B). Soil microbial enzymatic activities of dehydrogenase and FDA were enhanced due to the interaction of NPs with bacteria that promoted the growth of microorganisms, leading to the mobilization of nutrients and the breakdown of soil organic matter for maintaining soil fertility and nutrient recycling. The findings suggest that FeNPs and ZnNPs may act as co-factors for soil microbial enzymes, enhancing their metabolic activity, organic matter decomposition, and nutrient dynamics, which ultimately contribute to improving soil health and plant growth (Ameen et al., 2021; Ahmed et al., 2023).

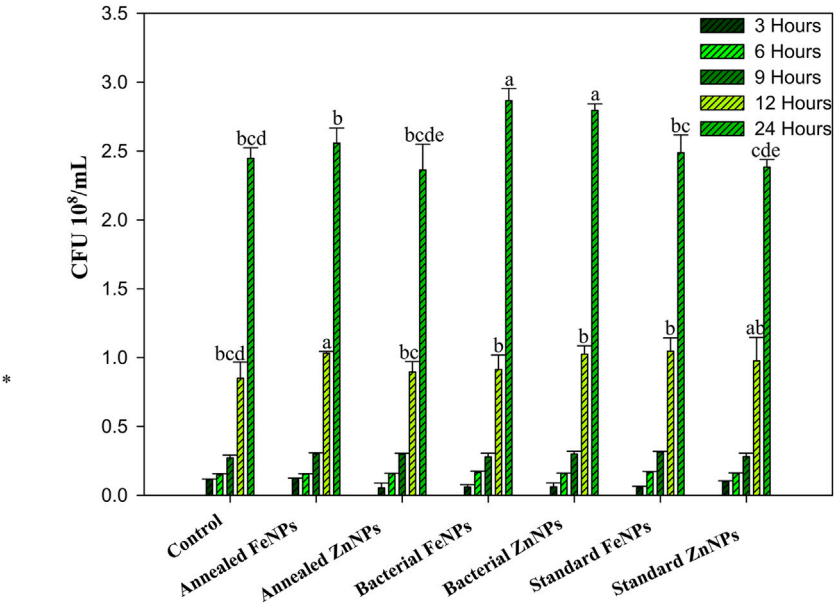

FIGURE 6
Effect of annealed Fe/ZnNPs (bacterial synthesized), bacterial Fe/ZnNPs (amorphous), and standard Fe/ZnNPs (chemical) on AW5 growth at different times (h). Error bars represent standard deviation, and different letters on the bar show significant differences ($p < 0.05$, $n = 3$).

3.6.2 Biochemical parameters

The effect of Fe and Zn NPs individually and in combination was observed on plant biochemical parameters, namely, chlorophyll and auxin (Figure 9). The chlorophyll content (μg/g) in leaf tissue ranged from 90.6 μg/g to 136 μg/g (Chl A) and from 42.2 μg/g to 87.4 μg/g (Chl B). The maximum increase was observed in treatment T9 (PGPR + ZnNPs + FeNPs, 100 ppm). Chl A and Chl B were increased by 51% and 107%, respectively, in T9 versus the RDF control (T2). The auxin content (μg/gm) ranged from 5.14 μg/gm to 8.16 μg/gm with a maximum increase in T15 (seed priming with PGPR + foliar application of ZnNPs-20 ppm). Auxin amount was increased by 59% in T15 versus the RDF control (T2), followed by T9 and T6 (up to 50%).

In a study performed by Seyed Sharifi et al., 2020, foliar application of FeNPs, ZnNPs (1,500 ppm), and their combination improved chlorophyll and auxin content in the plant via inducing the photosynthetic and plant metabolic pathways and significantly increased grain yield (22%, 11%, and 40%, respectively). A similar enhancing effect was recorded in our study using Fe and Zn NPs with increased chlorophyll levels and plant growth hormone (auxins). FeNP- and ZnNP-induced molecular pathways participate in electron transport chains, which especially involve photosystems I and II, thus improving ATP synthesis and overall energy efficiency for better plant growth and enhancement (Fallah et al., 2024; Qu et al., 2024). Auxins play an important role in plant growth, influencing cell elongation and division, and their enhancement is likely to contribute to the observed improvements in plant biomass and other growth traits. NPs generally showed a positive effect; the specific outcomes are dependent on the combination and concentration of NPs. Similarly, a significant enhancement in photosynthetic parameters (chlorophyll A, 45%, and B, 117%) was observed as a result of seed priming with FeNPs and ZnNPs (Rizwan et al., 2019). A dose-dependent effect of ZnNPs was reported via improving chlorophyll A (55%) and chlorophyll B (133%) at 50 ppm; a higher concentration (100 ppm) did not show a significant effect (Amooaghaie et al., 2017). The results are in line with our study, where an enhanced effect in plants treated with a 20 ppm dose of NPs versus 100 ppm was observed.

3.6.3 Plant physiological parameters

Wheat plants were uprooted after maturity, and physiological parameters (root and shoot length, plant biomass) were recorded (Figure 10). The shoot length ranged from 64.4 cm to 74.9 cm, with a maximum of 74.9 cm for treatment T4 (PGPR + FeNPs, 20 ppm) applied through seed priming, followed by T13 and T18. Shoot length was increased up to 8% in combination with NPs and PGPR versus the RDF control (T2). The root length ranged from 7.6 cm to 12.7 cm, with the maximum for T12, followed by T9, T10, and T11. There was an increase in root length (19%) in NP-treated seeds versus the RDF control (T2). The maximum plant biomass (14.9 g) was recorded in treatment T18 with an increase of 56% versus control (T2), followed by T10. The maximum 100 grains weight (6.4 g) was recorded in treatment T17 (seed priming with PGPR + foliar spray of Fe and Zn NPs (20 ppm), followed by T18 (6.02 g) versus the RDF control (T2). The grain weight was increased by 34% (T17) and 25% (T16).

The results of the present study, in the context of plant growth parameters, are similar to previous findings that demonstrated significant enhancement in key growth parameters with NP application. The interaction between bacteria and plant roots with NPs depends upon their characteristics, such as amorphous or crystallinity nature. The stability of crystalline NPs impacts the microbial community, whereas amorphous NPs discharge ions to modify bacterial functions and enzymatic processes. A similar effect with different doses of FeNPs and ZnNPs on plant growth attributes

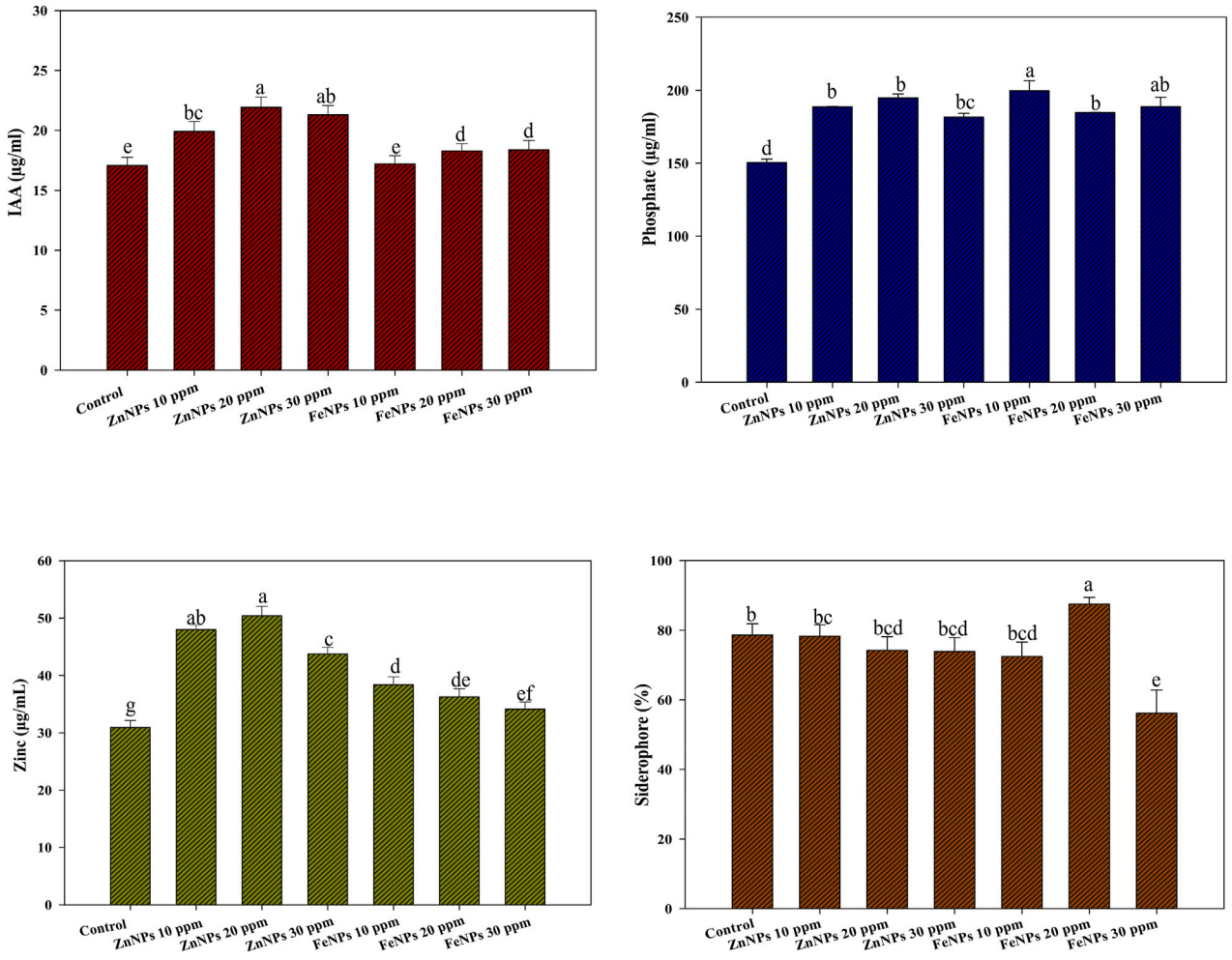

FIGURE 7
Effect of bacterial (amorphous) FeNPs and ZnNPs on plant growth-promoting traits of AW5. Error bars represent standard deviation, and different letters on the bar show significant differences ($p < 0.05$, $n = 3$).

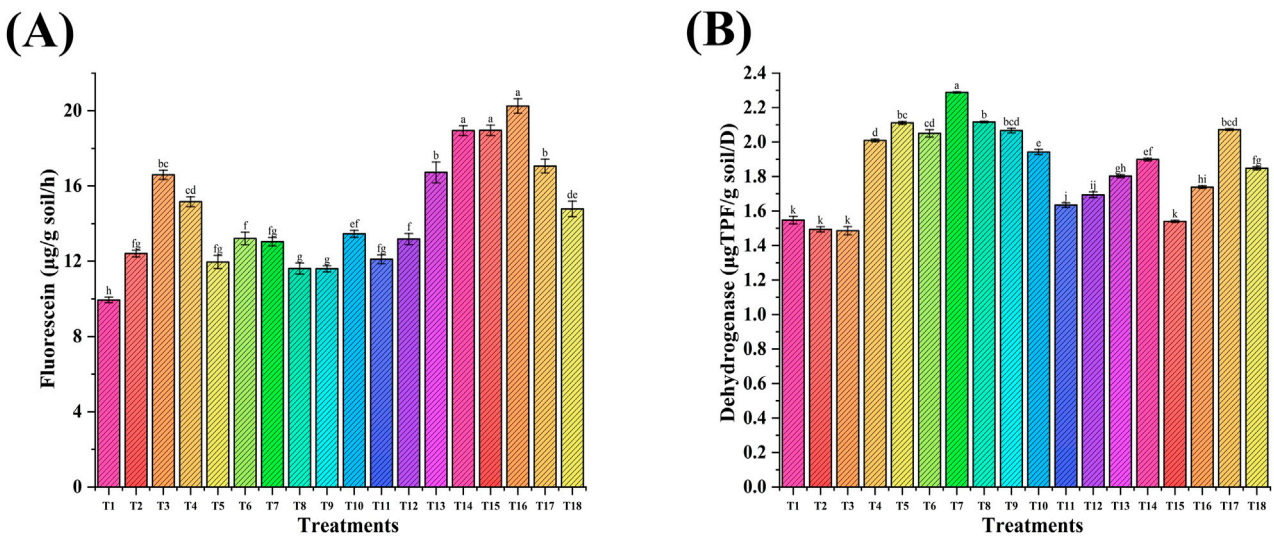

FIGURE 8
Effect of NP seed priming and foliar treatments on the soil microbial enzymatic activity: **(A)** Fluorescein diacetate and **(B)** dehydrogenase). Error bars represent standard deviation, and different letters on the bar show significant differences ($p < 0.05$, $n = 3$).

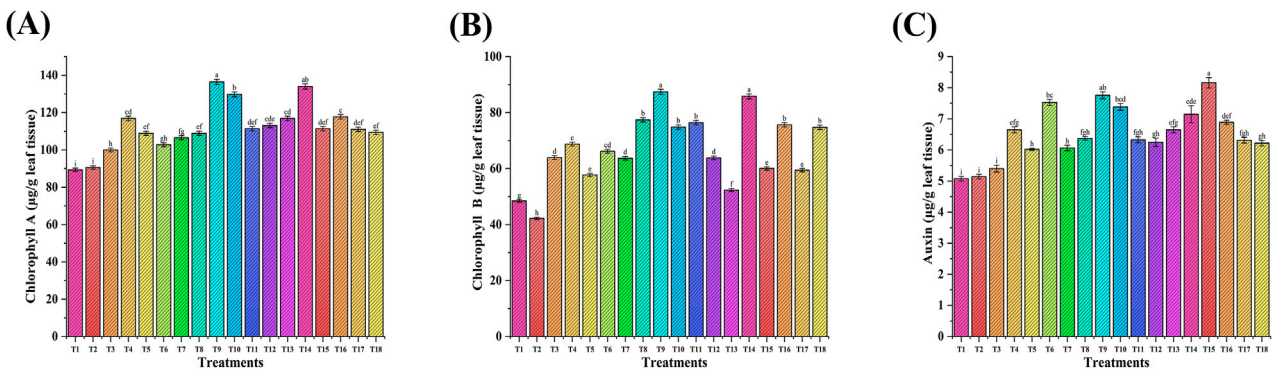

FIGURE 9
Effect of NP seed priming and foliar treatments on wheat biochemical parameters: **(A)** chlorophyll A; **(B)** chlorophyll B; and **(C)** auxin. Error bars represent standard deviation, and different letters on the bar show significant differences ($p < 0.05$, $n = 3$).

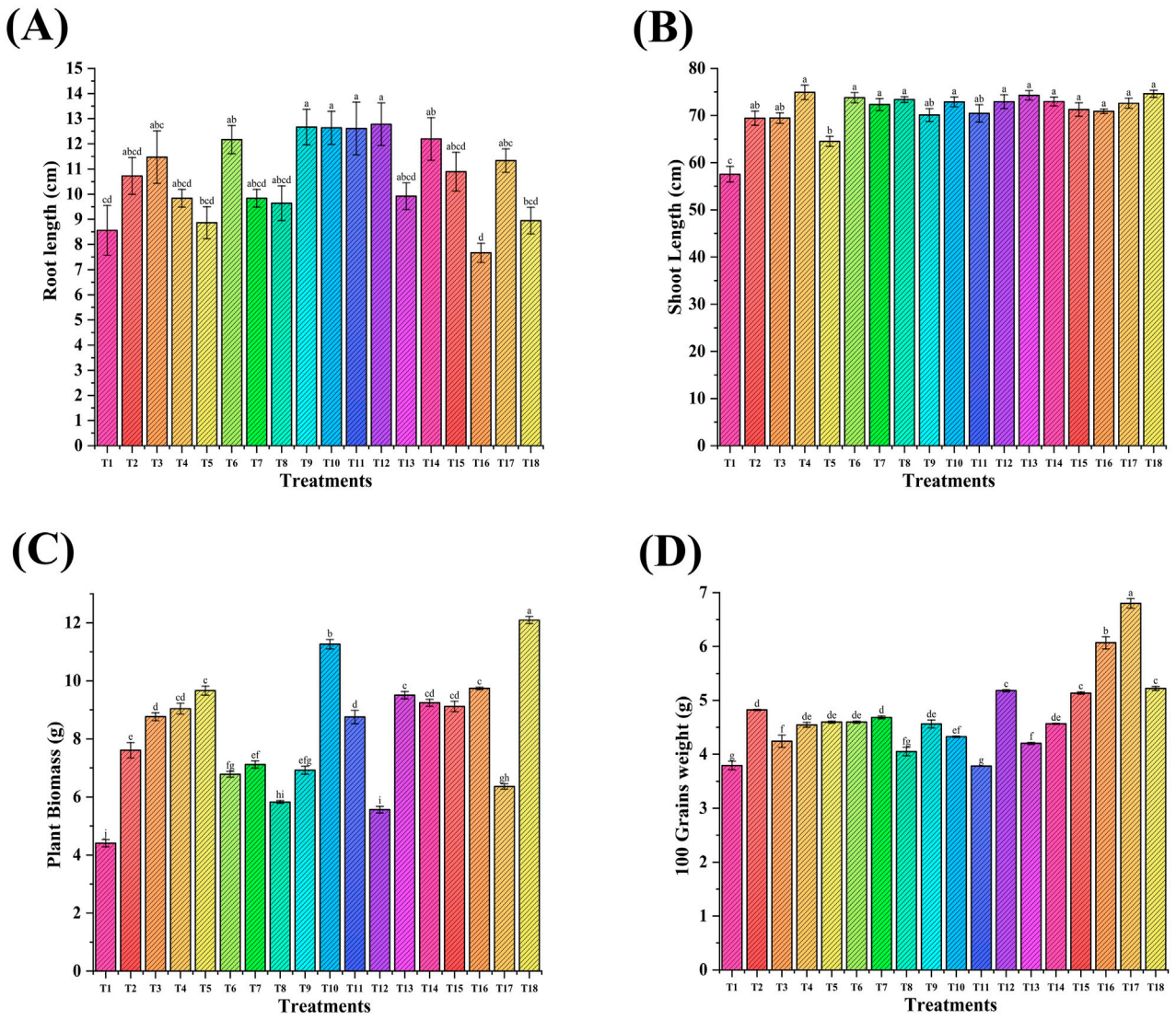

FIGURE 10
Effect of Fe and Zn NPs applied through seed priming and foliar treatments on wheat physiological parameters: **(A)** shoot length; **(B)** root length; **(C)** plant biomass; and **(D)** 100 grain weight. Error bars represent standard deviation, and different letters on the bar show significant differences ($p < 0.05$, $n = 3$).

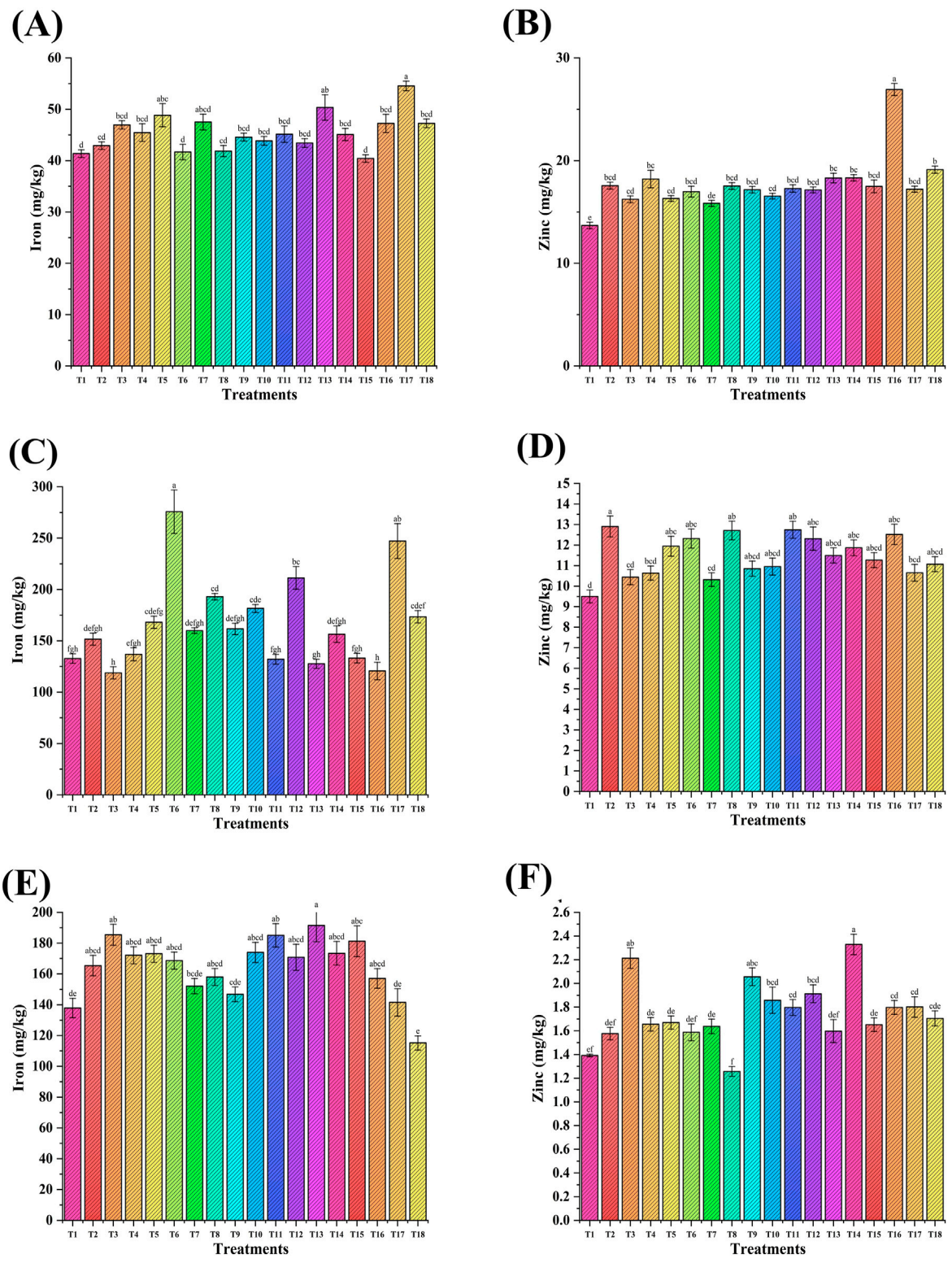

FIGURE 11
Effect of NP seed priming and foliar treatments on the nutritional content of wheat grain **(A,B)**, straw **(C,D)**, and soil **(E,F)**. Error bars represent standard deviation, and different letters on the bar show significant differences ($p < 0.05$, $n = 3$).

was reported. For example, seed priming of FeNPs and ZnNPs (20 ppm and 100 ppm) enhanced plant height by 37% and 35%, respectively, and other parameters such as shoot biomass (53%) and grain weight (74%) in all treatments containing NPs compared to the control (Rizwan et al., 2019). In another study, soil application with ZnNPs (20 ppm and 50 ppm) increased biomass (63%) and

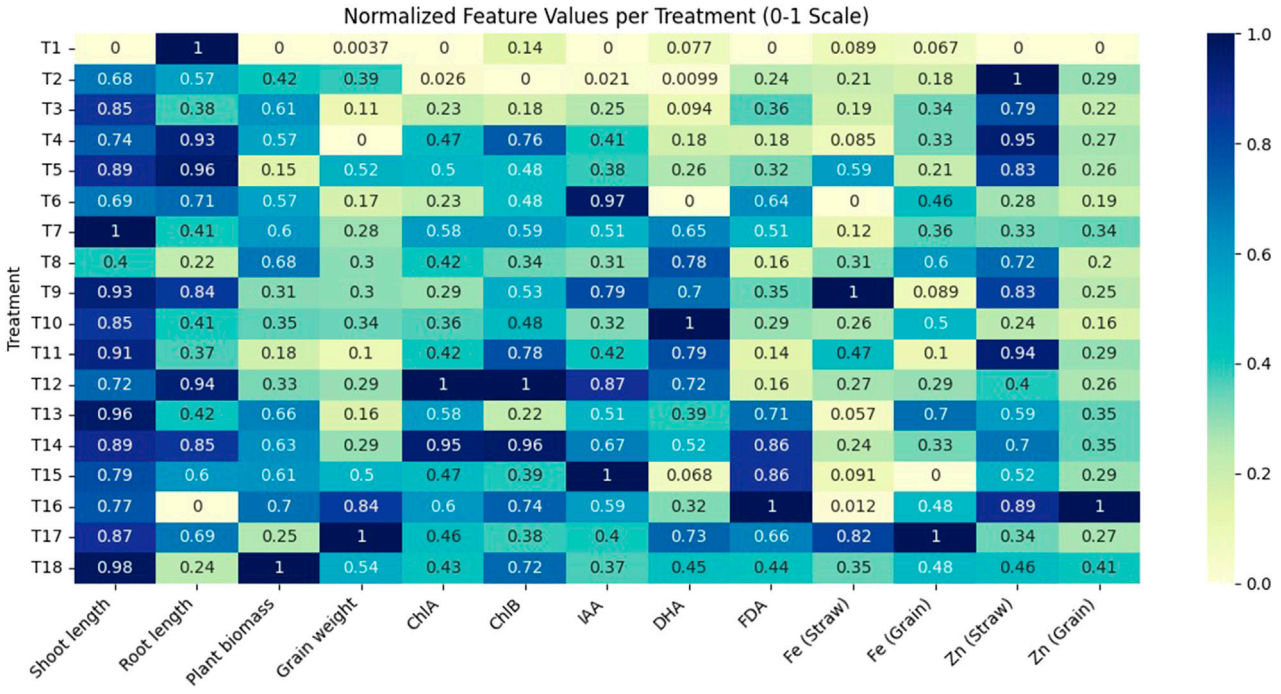

FIGURE 12
A correlation heatmap was generated using the seaborn library in Python to visualize the strength and direction of relationships between normalized features. The dataset was processed in the Google Colab, where leading and trailing whitespaces were removed and values normalized using Min–Max scaling (0–1 range). This ensured consistency across features and enhanced interpretability. The heatmap revealed both positive and negative correlations, aiding in feature selection and guiding further multivariate analysis.

grain yield (56%) (Du et al., 2019). Similarly, ZnNPs and zinc oxide (ZnO) increased wheat shoot fresh weight (up to 21% and 28%) with 100 ppm and 50 ppm, respectively. The application of bulk ZnNPs (50 ppm and 200 ppm) also increased root and shoot weight (Amooaghaie et al., 2017).

3.6.4 Effect of NPs on the nutritional content of wheat

The NP-induced micronutrient profiling of wheat and soil was studied (Figure 11). Iron (mg/kg) in wheat grains ranged from 40.4 mg/kg to 54.5 mg/kg (Figure 11A). The maximum increase of 27% was observed in the case of T17 (ZnNPs-20 ppm + FeNPs, 20 ppm foliar application + RDF and PGPR), followed by T13 (17%) versus the RDF control (T2). The iron content (ppm) in wheat straw ranged from 119 mg/kg to 276 mg/kg. The maximum increase of 82% was observed in T6 (seed priming-ZnNPs, 20 ppm, + RDF + PGPR), followed by T17 (63%) versus the RDF control (T2, Figure 11C). There was no significant increase in iron content in NP-treated soil versus the RDF control (T2, Figure 11E). The zinc content (mg/kg) in grain ranged from 15.8 mg/kg to 26.9 mg/kg (Figure 11B). The foliar application of NPs increased zinc content up to 53% (T16) versus the RDF control (T2). There was no significant increase of zinc in straw (Figure 11D). The zinc content (mg/kg) in soil ranged from 1.25 mg/kg to 2.32 mg/kg with a maximum rise of 48% in T14, followed by T3 (40%) and T9 (30%) versus the RDF control (T2, Figure 11F).

The manganese content in wheat grain increased up to 38% (T4 seed treatment) and 23% (T18 Foliar application) versus the RDF control (T2, Supplementary Figure S4B). Moreover, in the case of straw, an increase in Mn content was 47% (T4) and 55% (T6) applied via NP seed treatment and up to 15% (T17) through foliar application (Supplementary Figure S4D). NP treatments did not show any significant effect on soil manganese content versus the RDF control (T2, Supplementary Figure S4F). Copper content was increased up to 17% (T16) in wheat grains without any significant difference among the treatments (Supplementary Figure S4A). Moreover, Cu in soil (Supplementary Figure S4E) increased up to 83% (T14), followed by 46% (T3).

The combination of bacteria and NP could biofortify wheat crops to address the global challenge of hidden hunger. The biofortification of micronutrients (Fe, Cu, Zn, and Mn) and protein content in wheat under field conditions was reported in our previous study (Rana et al., 2012). Similarly, seed priming with FeNPs and ZnNPs enhanced the Zn and Fe content in plants and grains in other studies. Seed priming with Fe (10 ppm) and Zn (20 ppm) nanoparticles increased Fe and Zn in roots (28%), followed by shoots (18%) and grains (29%) versus the control (Rizwan et al., 2019). A distinct effect of bulk ZnO and ZnO NPs was reported on the increment of micronutrient content in wheat grain, straw, and soil (Amooaghaie et al., 2017).

3.6.5 Macronutrients

The phosphorus content in grains was significantly increased up to 25% (T16) and 7% (T4) when applied via foliar treatment and seed treatment, respectively, versus the RDF control (T2, Supplementary Figure S5A). In the case of straw, the P content

increased to 32% (T8 and T16) when applied through seed and foliar treatment of NPs versus the RDF control (T2, Supplementary Figure S5C). The soil P content was increased up to 47% (T9) and 40% (T14) through seed and foliar treatment, respectively, versus the RDF control (T2, Supplementary Figure S5E). The K content in grains was significantly increased up to 54% (T8) and 53% (T7) via seed treatment of NPs versus the RDF control (T2, Supplementary Figure S5B). In straw, the K content was increased up to 17% (T8 seed treatment) and 12% (T13 foliar spray, Supplementary Figure S5D). The soil K content was increased up to 12% (T9) and 16% (T14) through seed and foliar treatment of NPs, respectively, versus the RDF control (T2, Supplementary Figure S5F). FeNPs and ZnNPs enhanced translocation of metal ions through transport proteins combined with vascular sequestration processes, resulting in increased accumulation of nutrients in edible parts of the plant (Khan et al., 2021; Koç and Karayiğit, 2021; Sánchez-Palacios et al., 2023).

3.6.6 Proximate analysis of wheat grains

Seed carbohydrate and fat content in combination of PGPR and NPs increased up to 16% (T16) and 33% (T3), respectively, versus the RDF control (T2, Supplementary Figures S5A–C). The ash content in wheat grain increased up to 65% (T18-foliar spray) versus the RDF control (T2, Supplementary Figure S6B).

These results demonstrate the efficiency of NPs with PGPR to enhance nutrient content and metabolic pathways in bacteria for their better interaction with plants, leading to the biofortification of wheat in a sustainable manner. Wheat crop growth and yield were increased with the application of NPs (20 ppm and 100 ppm) through foliar application and seed priming. Moreover, wheat biofortification (nutrient content in wheat straw and grains) was achieved with NP treatment in combination with PGPR and correlated with all parameters and other studies (Figure 12; Supplementary Table S2). To explore the feasibility of the technology under field application, these NPs can be used with PGPR as a nanobiofertilizer through the seed treatment method. PGPR performed well in the root region, and their interaction with NPs bolsters plant growth hormones and the activity of bacterial soil enzymes that led to the mobilization of nutrients in the soil, making them available to the plant and biofortifying the crop.

4 Conclusion

Herein, the bacteria-assisted synthesis of iron and zinc nanoparticles (FeNPs and ZnNPs) was successfully performed in a sustainable manner. The NPs were biocompatible and showed negative polarity and colloidal stability. These bacterial FeNPs and ZnNPs proliferated the growth of PGPR and induced plant growth-promoting metabolites. The effect was significant at the optimized dose of Fe and Zn NPs (20 ppm). The results are corroborated by the increase in plant physiological parameters and biochemical properties, including biofortification of Fe and Zn in wheat. The NP treatment boosted soil health by multiplying soil microbial enzymatic activity and plant growth traits of PGPR. The impact of NPs on bacterial growth was dependent on type (bacterial/chemical), dose, and nature (crystalline and amorphous). Therefore, the optimization of the above-mentioned properties must be considered before any kind and scale (lab, pot, or field) of application in the agriculture sector to ensure safety and maximum impact on plant growth.

Our study demonstrates that bacterial FeNPs and ZnNPs can solve the toxicity issues associated with chemical NPs and agrochemicals (fertilizers). These characteristics strengthen the plant–microbe relationships through better nutrient acquisition and enhanced physiological traits of plants. These findings show together the biocompatibility and synergistic effects of FeNPs and ZnNPs on the biological activities of plant-beneficial rhizobacteria, emphasizing their possible use to support sustainable agricultural practices. The study addresses the sustainability development goals pertaining to zero hunger, sustainable growth, and food security.

Data availability statement

The original contributions presented in the study are included in the article/Supplementary Material, further inquiries can be directed to the corresponding authors.

Author contributions

PK: Software, Writing – original draft, Methodology, Project administration, Investigation. AR: Funding acquisition, Conceptualization, Writing – review and editing, Investigation, Writing – original draft, Resources, Validation, Project administration, Formal Analysis, Supervision, Data curation, Visualization, Methodology. MS: Software, Writing – review and editing, Methodology, Validation, Formal Analysis. SuK: Writing – review and editing. KC: Data curation, Writing – review and editing, Formal Analysis. UN: Formal Analysis, Writing – review and editing, Data curation. SaK: Writing – review and editing, Data curation, Validation, Formal Analysis. RD: Writing – review and editing, Data curation, Conceptualization, Resources, Investigation, Methodology, Project administration, Funding acquisition, Validation, Visualization, Writing – original draft, Supervision, Formal Analysis.

Funding

The author(s) declare that financial support was received for the research and/or publication of this article. Haryana State Council for Science Innovation and Technology (HSCSIT) provided financial support in terms of Project (HSCSIT/R&D/2023/2411, dated: 22/03/2023, and HSCSIT/R&D/2024/517, dated: 16/02/2024).

Conflict of interest

The authors declare that the research was conducted in the absence of any commercial or financial relationships that could be construed as a potential conflict of interest.

The author(s) declared that they were an editorial board member of Frontiers, at the time of submission. This had no impact on the peer review process and the final decision.

Generative AI statement

The author(s) declare that no Generative AI was used in the creation of this manuscript.

Publisher's note

All claims expressed in this article are solely those of the authors and do not necessarily represent those of their affiliated organizations, or those of the publisher, the editors and the reviewers. Any product that may be evaluated in this article, or claim that may be made by its manufacturer, is not guaranteed or endorsed by the publisher.

Supplementary material

The Supplementary Material for this article can be found online at: https://www.frontiersin.org/articles/10.3389/fnano.2025.1595252/full#supplementary-material

References

Ahmad, A., Mukherjee, P., Senapati, S., Mandal, D., Khan, M. I., Kumar, R., et al. (2003). Extracellular biosynthesis of silver nanoparticles using the fungus *Fusarium oxysporum*. *Colloids Surfaces B Biointerfaces* 28, 313–318. doi:10.1016/S0927-7765(02)00174-1

Ahmed, A., He, P. P., He, P. P., Wu, Y., He, Y., and Munir, S. (2023). Environmental effect of agriculture-related manufactured nano-objects on soil microbial communities. *Environ. Int.* 173, 107819. doi:10.1016/j.envint.2023.107819

Alban, L. A., and Kellogg, M. (1959). Methods of soil analysis as used in the OSC soil testing laboratory. Available online at: https://ir.library.oregonstate.edu/downloads/db78td03c.

Ameen, F., Alsamhary, K., Alabdullatif, J. A., and Alnadhari, S. (2021). A review on metal-based nanoparticles and their toxicity to beneficial soil bacteria and fungi. *Ecotoxicol. Environ. Saf.* 213, 112027. doi:10.1016/j.ecoenv.2021.112027

Amooaghaie, R., Norouzi, M., and Saeri, M. (2017). Impact of zinc and zinc oxide nanoparticles on the physiological and biochemical processes in tomato and wheat. *Botany* 95, 441–455. doi:10.1139/cjb-2016-0194

Bhutani, N., Maheshwari, R., Kumar, P., Dahiya, R., and Suneja, P. (2021). Bioprospecting for extracellular enzymes from endophytic bacteria isolated from *Vigna radiata* and *Cajanus cajan*. *J. Appl. Biol. Biotechnol.* 9, 2–4. doi:10.7324/jabb.2021.9304

Butaite, E., Baumgartner, M., Wyder, S., and Kümmerli, R. (2017). Siderophore cheating and cheating resistance shape competition for iron in soil and freshwater *Pseudomonas* communities. *Nat. Commun.* 8, 1–12. doi:10.1038/s41467-017-00509-4

Campaña, A. L., Saragliadis, A., Mikheenko, P., and Linke, D. (2023). Insights into the bacterial synthesis of metal nanoparticles. *Front. Nanotechnol.* 5, 1216921. doi:10.3389/fnano.2023.1216921

Chatterjee, S., Bandyopadhyay, A., and Sarkar, K. (2011). Effect of iron oxide and gold nanoparticles on bacterial growth leading towards biological application. *J. Nanobiotechnology* 9, 34–37. doi:10.1186/1477-3155-9-34

Crespo, K. A., Baronetti, J. L., Quinteros, M. A., Páez, P. L., and Paraje, M. G. (2017). Intra- and extracellular biosynthesis and characterization of iron nanoparticles from prokaryotic microorganisms with anticoagulant activity. *Pharm. Res.* 34, 591–598. doi:10.1007/s11095-016-2084-0

Dehkordi, H. A., Dastafkan, K., Moshaii, A., and Mokhtari, A. (2015). Thermal post-annealing and gas concentration effect on liquid petroleum gas sensing characteristics of nanocrystalline zinc oxide thin films. *J. Mater. Sci. Mater. Electron.* 26, 3134–3142. doi:10.1007/s10854-015-2808-7

Di Simine, C. D., Sayer, J. A., and Gadd, G. M. (1998). Solubilization of zinc phosphate by a strain of *Pseudomonas fluorescens* isolated from a forest soil. *Biol. Fertil. Soils* 28, 87–94. doi:10.1007/s003740050467

Du, W., Yang, J., Peng, Q., Liang, X., and Mao, H. (2019). Comparison study of zinc nanoparticles and zinc sulphate on wheat growth: from toxicity and zinc biofortification. *Chemosphere* 227, 109–116. doi:10.1016/j.chemosphere.2019.03.168

El-Naggar, N. E. A., and Abdelwahed, N. A. M. (2014). Application of statistical experimental design for optimization of silver nanoparticles biosynthesis by a nanofactory *Streptomyces viridochromogenes*. *J. Microbiol.* 52, 53–63. doi:10.1007/s12275-014-3410-z

Eltarahony, M., Zaki, S., Elkady, M., and Abd-El-Haleem, D. (2018). Biosynthesis, characterization of some combined nanoparticles, and its biocide potency against a broad spectrum of pathogens. *J. Nanomater.* 2018, 1–16. doi:10.1155/2018/5263814

Fallah, S., Yusefi-Tanha, E., and Peralta-Videa, J. R. (2024). Interaction of nanoparticles and reactive oxygen species and their impact on macromolecules and plant production. *Plant Nano Biol.* 10, 100105. doi:10.1016/j.plana.2024.100105

Farahmandjou, M., and Soflaee, F. (2015). Synthesis and characterization of α-Fe2O3 nanoparticles by simple co-precipitation method. *Phys. Chem. Res.* 3, 191–196. doi:10.22036/pcr.2015.9193

González-Melendi, P., Fernández-Pacheco, R., Coronado, M. J., Corredor, E., Testillano, P. S., Risueño, M. C., et al. (2008). Nanoparticles as smart treatment-delivery systems in plants: assessment of different techniques of microscopy for their visualization in plant tissues. *Ann. Bot.* 101, 187–195. doi:10.1093/aob/mcm283

Gopinath, V., Priyadarshini, S., Loke, M. F., Arunkumar, J., Marsili, E., MubarakAli, D., et al. (2017). Biogenic synthesis, characterization of antibacterial silver nanoparticles and its cell cytotoxicity. *Arab. J. Chem.* 10, 1107–1117. doi:10.1016/j.arabjc.2015.11.011

Green, V. S., Stott, D. E., and Diack, M. (2006). Assay for fluorescein diacetate hydrolytic activity: optimization for soil samples. *Soil Biol. biochem.* 38, 693–701. doi:10.1016/j.soilbio.2005.06.020

Guardiola-Márquez, C. E., López-Mena, E. R., Segura-Jiménez, M. E., Gutierrez-Marmolejo, I., Flores-Matzumiya, M. A., Mora-Godínez, S., et al. (2023). Development and evaluation of zinc and iron nanoparticles functionalized with plant growth-promoting rhizobacteria (PGPR) and microalgae for their application as bio-nanofertilizers. *Plants* 12, 3657. doi:10.3390/plants12203657

He, H., Cao, J., Fei, X., and Duan, N. (2019). High-temperature annealing of ZnO nanoparticles increases the dissolution magnitude and rate in water by altering O vacancy distribution. *Environ. Int.* 130, 104930. doi:10.1016/j.envint.2019.104930

Huang, L., Bell, R. W., Dell, B., and Woodward, J. (2004). Rapid nitric acid digestion of plant material with an open-vessel microwave system. *Commun. Soil Sci. Plant Anal.* 35, 427–440. doi:10.1081/css-120029723

Iqtedar, M., Riaz, H., Kaleem, A., Abdullah, R., Aihetasham, A., Naz, S., et al. (2020). Biosynthesis, optimization and characterization of ZnO nanoparticles using *Bacillus cereus* MN181367 and their antimicrobial activity against multidrug resistant. *Rev. Mex. Ing. Quím.* 19, 253–266. doi:10.24275/rmiq/bio1605

Kalpana, V. N., Kataru, B. A. S., Sravani, N., Vigneshwari, T., Panneerselvam, A., and Devi Rajeswari, V. (2018). Biosynthesis of zinc oxide nanoparticles using culture filtrates of *Aspergillus niger*: antimicrobial textiles and dye degradation studies. *OpenNano* 3, 48–55. doi:10.1016/j.onano.2018.06.001

Kaur, H., Kalia, A., and Manchanda, P. (2024). Elucidating the effect of TiO2 nanoparticles on mung bean rhizobia via in vitro assay: Influence on growth, morphology, and plant growth promoting traits. *J. Basic Microbiol.* 64, 2300306. doi:10.1002/JOBM.202300306

Khan, M. K., Pandey, A., Hamurcu, M., Gezgin, S., Athar, T., Rajput, V. D., et al. (2021). Insight into the prospects for nanotechnology in wheat biofortification. *Biol* 10, 1123–10. doi:10.3390/biology10111123

Khan, M. R., Fromm, K. M., Rizvi, T. F., Giese, B., Ahamad, F., Turner, R. J., et al. (2020). Metal nanoparticle–microbe interactions: synthesis and antimicrobial effects. *Part. Part. Syst. Charact.* 37, 1900419. doi:10.1002/ppsc.201900419

Koç, E., and Karayiğit, B. (2021). Assessment of biofortification approaches used to improve micronutrient-dense plants that are a sustainable solution to combat hidden hunger. *J. Soil Sci. Plant Nutr.* 22, 475–500. doi:10.1007/S42729-021-00663-1

Kouhbanani, M. A. J., Beheshtkhoo, N., Taghizadeh, S., Amani, A. M., and Alimardani, V. (2019). One-step green synthesis and characterization of iron oxide nanoparticles using aqueous leaf extract of *Teucrium polium* and their catalytic application in dye degradation. *Adv. Nat. Sci. Nanosci. Nanotechnol.* 10, 015007. doi:10.1088/2043-6254/AAFE74

Kumar, A., Rishabh, N., Singh, N., Gautam, Y. K., Priya, N., and Malik, N. (2025). Valorizing banana peel waste into mesoporous biogenic nanosilica and novel nano-biofertilizer formulation thereof via nano-biopriming inspired tripartite interaction studies. *ACS Omega* 10, 5537–5553. doi:10.1021/acsomega.4c08152

Kumar, P., Sudesh, Kumar, A., and Suneja, P. (2022). Studies on the physicochemical parameter's optimization for indole-3-acetic acid production by Pantoea agglomerans CPHN2 using one factor at a time (OFAT) and response surface methodology (RSM). *Environ. Sustain* 6, 35–44. doi:10.1007/s42398-022-00254-5

Kumaravel, J., Lalitha, K., Arunthirumeni, M., and Shivakumar, M. S. (2021). Mycosynthesis of bimetallic zinc oxide and titanium dioxide nanoparticles for

control of *Spodoptera frugiperda*. *Pestic. Biochem. Physiol.* 178, 104910. doi:10.1016/j.pestbp.2021.104910

Liu, J., Vipulanandan, C., Cooper, T. F., and Vipulanandan, G. (2013). Effects of Fe nanoparticles on bacterial growth and biosurfactant production. *J. Nanoparticle Res.* 15, 1405–1413. doi:10.1007/s11051-012-1405-4

Maheshwari, R., Bhutani, N., and Suneja, P. (2019). Screening and characterization of siderophore producing endophytic bacteria from *Cicer arietinum* and *Pisum sativum* plants. *J. Appl. Biol. Biotechnol.* 7, 7–14. doi:10.7324/jabb.2019.70502

Maheshwari, R., Kumar, P., Bhutani, N., and Suneja, P. (2022). Exploration of plant growth-promoting endophytic bacteria from *Pisum sativum* and *Cicer arietinum* from South–West Haryana. *J. Basic Microbiol.* 62, 857–874. doi:10.1002/jobm.202100575

Majeed, S., Danish, M., Mohamad Ibrahim, M. N., Sekeri, S. H., Ansari, M. T., Nanda, A., et al. (2021). Bacteria mediated synthesis of iron oxide nanoparticles and their antibacterial, antioxidant, cytocompatibility properties. *J. Clust. Sci.* 32, 1083–1094. doi:10.1007/s10876-020-01876-7

Manna, M., Rengasamy, B., and Sinha, A. K. (2024). A rapid and robust colorimetric method for measuring relative abundance of auxins in plant tissues. *Phytochem. Anal.* 35, 1052–1062. doi:10.1002/pca.3340

Mathur, P., Saini, S., Paul, E., Sharma, C., and Mehtani, P. (2021). Endophytic fungi mediated synthesis of iron nanoparticles: characterization and application in methylene blue decolorization. *Curr. Res. Green Sustain. Chem.* 4, 100053. doi:10.1016/j.crgsc.2020.100053

Menazea, A. A., Ismail, A. M., and Samy, A. (2021). Novel green synthesis of zinc oxide nanoparticles using orange waste and its thermal and antibacterial activity. *J. Inorg. Organomet. Polym. Mater.* 31, 4250–4259. doi:10.1007/s10904-021-02074-2

Mukherjee, P., Ahmad, A., Mandal, D., Senapati, S., Sainkar, S. R., Khan, M. I., et al. (2001). Fungus-mediated synthesis of silver nanoparticles and their immobilization in the mycelial matrix: a novel biological approach to nanoparticle synthesis. *Nano Lett.* 1, 515–519. doi:10.1021/nl0155274

Nandhini, M., Rajini, S. B., Udayashankar, A. C., Niranjana, S. R., Lund, O. S., Shetty, H. S., et al. (2019). Biofabricated zinc oxide nanoparticles as an eco-friendly alternative for growth promotion and management of downy mildew of pearl millet. *Crop Prot.* 121, 103–112. doi:10.1016/j.cropro.2019.03.015

Omajali, J. B., Mikheenko, I. P., Merroun, M. L., Wood, J., and Macaskie, L. E. (2015). Characterization of intracellular palladium nanoparticles synthesized by *Desulfovibrio desulfuricans* and *Bacillus benzeovorans*. *J. Nanoparticle Res.* 17, 1–17. doi:10.1007/s11051-015-3067-5/figures/5

Payne, S. M. (1994). Detection, isolation, and characterization of siderophores. *Methods Enzymol.* 235, 329–344. doi:10.1016/0076-6879(94)35151-1

Pikovskaya, R. I. (1948). Mobilization of phosphorus in soil in connection with the vital activity of some microbial species. *Mikrobiologiya* 17, 362–370.

Prischl, M., Hackl, E., Pastar, M., Pfeiffer, S., and Sessitsch, A. (2012). Genetically modified Bt maize lines containing cry3Bb1, cry1A105 or cry1Ab2 do not affect the structure and functioning of root-associated endophyte communities. *Appl. Soil Ecol.* 54, 39–48. doi:10.1016/j.apsoil.2011.12.005

Qu, R., Liu, N., Wen, Q., Guo, J., and Ge, F. (2024). Molecular mechanism of dissolvable metal nanoparticles-enhanced CO2 fixation by algae: metal-chlorophyll synthesis. *Environ. Pollut.* 349, 123987. doi:10.1016/j.envpol.2024.123987

Rana, A., Joshi, M., Prasanna, R., Shivay, Y. S., and Nain, L. (2012). Biofortification of wheat through inoculation of plant growth promoting rhizobacteria and cyanobacteria. *Eur. J. Soil Biol.* 50, 118–126. doi:10.1016/j.ejsobi.2012.01.005

Rana, A., Saharan, B., Joshi, M., Prasanna, R., Kumar, K., and Nain, L. (2011). Identification of multi-trait PGPR isolates and evaluating their potential as inoculants for wheat. *Ann. Microbiol.* 61, 893–900. doi:10.1007/s13213-011-0211-z

Rana, A., Yadav, K., and Jagadevan, S. (2020). A comprehensive review on green synthesis of nature-inspired metal nanoparticles: mechanism, application and toxicity. *J. Clean. Prod.* 272, 122880. doi:10.1016/j.jclepro.2020.122880

Rizwan, M., Ali, S., Ali, B., Adrees, M., Arshad, M., Hussain, A., et al. (2019). Zinc and iron oxide nanoparticles improved the plant growth and reduced the oxidative stress and cadmium concentration in wheat. *Chemosphere* 214, 269–277. doi:10.1016/j.chemosphere.2018.09.120

Sánchez-Palacios, J. T., Henry, D., Penrose, B., and Bell, R. (2023). Formulation of zinc foliar sprays for wheat grain biofortification: a review of current applications and future perspectives. *Front. Plant Sci.* 14, 1247600. doi:10.3389/fpls.2023.1247600

Schwyn, B., and Neilands, J. B. (1987). Universal chemical assay for the detection and determination of siderophores. *Anal. Biochem.* 160, 47–56. doi:10.1016/0003-2697(87)90612-9

Seyed Sharifi, R., Khalilzadeh, R., Pirzad, A., and Anwar, S. (2020). Effects of biofertilizers and nano zinc-iron oxide on yield and physicochemical properties of wheat under water deficit conditions. *Commun. Soil Sci. Plant Anal.* 51, 2511–2524. doi:10.1080/00103624.2020.1845350

Shang, Y., Kamrul Hasan, M., Ahammed, G. J., Li, M., Yin, H., and Zhou, J. (2019). Applications of nanotechnology in plant growth and crop protection: a review. *Molecules* 24, 2558. doi:10.3390/molecules24142558

Shankar, P. D., Shobana, S., Karuppusamy, I., Pugazhendhi, A., Ramkumar, V. S., Arvindnarayan, S., et al. (2016). A review on the biosynthesis of metallic nanoparticles (gold and silver) using bio-components of microalgae: formation mechanism and applications. *Enzyme Microb. Technol.* 95, 28–44. doi:10.1016/j.enzmictec.2016.10.015

Shelar, A., Nile, S. H., Singh, A. V., Rothenstein, D., Bill, J., Xiao, J., et al. (2023). Recent advances in nano-enabled seed treatment strategies for sustainable agriculture: challenges, risk assessment, and future perspectives. *Nano-Micro Lett.* 15, 54–37. doi:10.1007/S40820-023-01025-5

Shukla, S., Jadaun, A., Arora, V., Sinha, R. K., Biyani, N., and Jain, V. K. (2015). *In vitro* toxicity assessment of chitosan oligosaccharide coated iron oxide nanoparticles. *Toxicol. Rep.* 2, 27–39. doi:10.1016/j.toxrep.2014.11.002

Sundararaju, S., Arumugam, M., and Bhuyar, P. (2020). *Microbacterium* sp. MRS-1, a potential bacterium for cobalt reduction and synthesis of less/non-toxic cobalt oxide nanoparticles (Co3O4). *Beni-Suef Univ. J. Basic Appl. Sci.* 9, 44–49. doi:10.1186/s43088-020-00070-y

Takeshita, V., Campos, E. V. R., Rodrigues, J. S., and Fraceto, L. F. (2023). Opinion: hybrid nanoparticle systems – two-way delivery approach for agriculture. *Plant Nano Biol.* 6, 100053. doi:10.1016/j.plana.2023.100053

Tang, Y. W., and Bonner, J. (1948). The enzymatic inactivation of indole acetic acid; the physiology of the. *Am. J. Bot.* 35, 570–578. doi:10.1002/j.1537-2197.1948.tb08123.x

Thalmann, A. (1968). Zur methodik der bestimmung der dehydrogenaseaktivitat im boden mittels triphenytetrazoliumchlorid (TTC). *Landwirtsch. Forsch.* 21, 249–258.

Tikariha, S., Banerjee, S., Dev, A., and Singh, S. (2017). Growth phase-dependent synthesis of gold nanoparticles using *Bacillus licheniformis*. *Appl. Biotechnol. Sustain. Dev.*, 121–128. doi:10.1007/978-981-10-5538-6_15

Timmusk, S., Seisenbaeva, G., and Behers, L. (2018). Titania (TiO2) nanoparticles enhance the performance of growth-promoting rhizobacteria. *Sci. Rep.* 8, 617–13. doi:10.1038/s41598-017-18939-x

Wellburn, A. R. (1994). The spectral determination of chlorophylls A and B, as well as total carotenoids, using various solvents with spectrophotometers of different resolution. *J. Plant Physiol.* 144, 307–313. doi:10.1016/S0176-1617(11)81192-2

Xia, X., Wu, S., Li, N., Wang, D., Zheng, S., and Wang, G. (2018). Novel bacterial selenite reductase CsrF responsible for Se(IV) and Cr(VI) reduction that produces nanoparticles in *Alishewanella* sp. WH16-1. *J. Hazard. Mater.* 342, 499–509. doi:10.1016/j.jhazmat.2017.08.051

Zaki, S. A. E. F., Kamal, A., Ashmawy, N. A., and Shoeib, A. A. (2021). Nano-metals forming bacteria in Egypt. I. synthesis, characterization and effect on some phytopathogenic bacteria *in vitro*. *Sci. Rep.* 11, 12876–18. doi:10.1038/s41598-021-92171-6

Zhang, H., Wang, R., Chen, Z., Cui, P., Lu, H., Yang, Y., et al. (2021). The effect of zinc oxide nanoparticles for enhancing rice (*Oryza sativa* l.) yield and quality. *Agriculture* 11, 1247. doi:10.3390/agriculture11121247